ACS APPLIED MATERIALS & INTERFACES

www.acsami.org
Research Article

Enzyme Reactions Are Accelerated or Decelerated When the Enzymes Are Located Near the DNA Nanostructure

Peng Lin, Tomohiko Hayashi, Huyen Dinh, Eiji Nakata, Masahiro Kinoshita, and Takashi Morii*

Cite This: ACS Appl. Mater. Interfaces 2025, 17, 15775−15792

ABSTRACT: It is known experimentally that enzymatic reactions are often accelerated when the enzymes are assembled on the scaffold of DNA nanostructures. However, the exact mechanism by which this acceleration occurs remains unclear. Here, we study the reactions of enzymes with different catalytic mechanisms assembled on a DNA scaffold with various substrates. Analysis of the hydration properties of the substrates using our accurate statistical mechanics theory classifies the substrates into two groups that behave as hydrophilic and hydrophobic solutes, respectively. The reaction of the enzyme on the DNA scaffold is accelerated with a hydrophilic substrate but decelerated with a hydrophobic substrate. We propose a mechanism of acceleration or deceleration in which, due to the formation of a high-density layer of water near the DNA surface with high negative charge density, the concentration of a substrate with high energetic affinity for water within the layer becomes higher than that near a free enzyme, whereas that of a substrate with low energetic affinity becomes lower within the layer. This study provides chemical and physical insights into a general case of biocatalysts, where the rates of chemical reactions occurring at the interface of biomolecules in aqueous environments can differ substantially from those in the bulk solution due to variations in the local concentration of a given ligand.

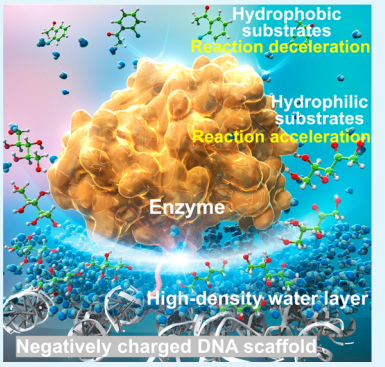

KEYWORDS: *biocatalyst, DNA scaffold, enzyme reaction, hydration, interface*

1. INTRODUCTION

The high efficiency and specificity of stepwise biochemical transformations by metabolic cascade reactions in the cell are thought to depend on the spatial organization of enzymes assembled on specific scaffolds, such as membranes or proteins.[1,2] The thylakoid membrane carries the photosynthetic and respiratory electron transport components to simultaneously conduct oxygenic photosynthesis and respiration.[3] Mammalian cytochrome P450 anchored on the membrane of endoplasmic reticulum is involved in the biotransformation of many endo- and exogenous compounds.[4] In addition to the membranes, the polyhedral protein shells of carboxysome encapsulate ribulose 1,5-bisphosphate carboxylase/oxygenase and carbonic anhydrase, which carry out the critical step of carbon fixation.[5] While scaffolds in nature have been proposed to support the colocalization of enzymes and promote enzymatic functions, the effect of the scaffold itself on the catalytic reaction of individual enzymes remains unclear.

To mimic natural scaffold systems, reactions of single or multiple enzymes on various carriers such as liposomes, polymersomes, proteins, and nucleic acid−based materials have been studied.[6] Among these, macromolecular scaffolds constructed using DNA nanostructures, DNA scaffolds, have attracted great interest because of their structural programmability and precise addressability.[7] With these advantages, biomolecules can be assembled on the DNA scaffold with a precise control over the locations and numbers. DNA scaffolds have been applied in the field of biosensing, drug delivery, diagnosis, and biocatalysts.[8]

A variety of enzymes with different mechanisms have been reported to exhibit kinetic enhancements when assembled on the DNA nanostructure,[9] but a common mechanism underlying these observations remains to be elucidated.[10] A role for highly charged DNA scaffolds in catalytic enhancement of DNA-tethered enzymes has been proposed by increasing the local concentration of substrate at the surface of the DNA scaffold through electrostatic interaction,[11−13] or by reducing the adsorption of the scaffolded enzyme to the surface of the reaction vessel, thereby deactivating the enzymes,[14] or by modulating a lower local pH in the vicinity of enzymes.[15] In addition, Zhao et al. hypothesized that the activity of enzymes individually encapsulated in DNA cages is enhanced by the stabilization of the enzyme structure by a highly ordered, hydrogen-bonded water environment originating from the DNA surface.[16]

In our previous study, xylose reductase (XR) and xylitol dehydrogenase (XDH), both derived from the D-xylose

Received: October 21, 2024
Revised: December 26, 2024
Accepted: February 3, 2025
Published: March 2, 2025

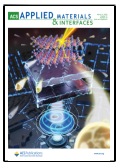

pathway, were individually assembled on the fully open state of a DNA hexagonal prism[17] to increase the reaction rate of both XR and XDH. Because XR and XDH have different pH preferences, at pH 6 and 8, respectively, and the charge of their substrates is neutral, our results indicate that neither the previous proposals of substrate attraction to the DNA scaffold by electrostatic interaction[11−13] nor the lower local pH at the DNA scaffold surface[15] is the general factor responsible for the increase in enzyme reaction rate. The effect of the water environment near the DNA surface[16] is a likely candidate. However, it is not the simple stabilization of the enzyme structure, but the specific stabilization of the transition state that accelerates the enzyme reaction. Furthermore, the relationship between the water environment surrounding the enzyme and the stabilization of the enzyme structure is unclear. While the reduced adsorption of enzymes on the surface of the reaction vessel when loaded onto the DNA scaffold would contribute in part to the accelerated reaction,[14] the critical and general properties of the DNA scaffold that enhance a variety of enzyme reactions with different catalytic mechanisms remain to be elucidated.

In this study, we unveil a common mechanism underlying these observations for the DNA-scaffolded enzymes that acts on enzymes independent of their catalytic mechanisms. By testing a variety of substrates with XR and carbonic anhydrase (CA), we found that the reaction of the enzyme on the DNA scaffold can be accelerated or slowed down, depending on the substrate properties. Due to the strong electrostatic attraction between the negative charge of the DNA surface and the dipole moment in a water molecule, a high-density layer of water is formed near the surface of the DNA scaffold. Hydrophilic substrates are enriched within the layer, while hydrophobic substrates are diluted within the layer, where hydrophilicity or hydrophobicity can be judged not by the conventional log P measure, but by whether the hydration free energy of the substrate, calculated using our accurate statistical mechanics theory developed by Kinoshita and co-workers,[18] is lower or higher than that of a water molecule. Consequently, the substrate concentration near an enzyme in the vicinity of the DNA surface is higher and lower than that near a free enzyme for hydrophilic and hydrophobic substrates, respectively. This study provides original insights into the origins of the reaction acceleration for DNA-scaffolded enzymes compared to the corresponding free enzymes and suggests novel roles for the cellular protein scaffolds and lipid membranes in enzymatic reactions.

2. EXPERIMENT SECTION

2.1. Materials. The single-stranded M13mp18 viral DNA (7249) was purchased from Guild Biosciences. BG-GLA-NHS (S9151S) and Bovine Serum Albumin (BSA, BS9000S) were purchased from New England Biolabs. Purified DNA origami staple strands, and all other oligonucleotides were obtained from Sigma-Aldrich (St. Louis, MO), Japan Bio Services Co., LTD (Saitama, Japan) or Thermo Fisher Scientific (Tokyo, Japan). β-Nicotinamide adenine dinucleotide in reduced form (β-NADH) was obtained from Oriental Yeast (Tokyo, Japan). 4-nitrobenzaldehyde, ethyl benzoylformate and *o*-chloroacetophenone were purchased from Sigma-Aldrich (St. Louis, MO). D,L-glyceraldehyde was purchased from Nacalai Tesque (Kyoto, Japan). *p*-nitrophenyl acetate (*p*-NPA), *p*-nitrophenyl butyrate (*p*-NPB) and *p*-nitrophenyl valerate (*p*-NPV) were purchased from Sigma-Aldrich and used without further purification. The Log P values were calculated using ChemDraw (version 17.1, PerkinElmer). Sephacryl S-400 was purchased from GE Healthcare Japan Inc. (Tokyo, Japan). Toyopearl HW-55F was purchased from Tosoh Bioscience GmbH (Griesheim, Germany). Ultrafree-MC-DV column and Amicon Ultra-0.5 Centrifugal Filter Device (100 kDa) were obtained from Merckmillipore (Darmstadt, Germany). Low-binding microtube (BT-150L, 1.5 mL, nonpyrogenic & RNase-/DNase- free) was purchased from Ina OPTIKA CO., LTD (Osaka, Japan). D-xylose, and all other chemicals and reagents were purchased from Wako Chemicals (Tokyo, Japan) or Nacalai Tesque (Kyoto, Japan).

2.2. Assembly of Enzymes on the DNA Scaffolds. *2.2.1. Preparation of DNA Origami Scaffolds.* The fully open state of the three-dimensional DNA hexagonal prism was constructed as previously described.[17,19,20] A mixture (50 μL) containing M13mp18 (20 nM) and staple DNA strands (10 equiv, 200 nM) in a DNA scaffold folding buffer (pH 8.0) containing 5 mM Tris-HCl, 1 mM EDTA and 8 mM $MgCl_2$, was subjected to a thermal-annealing ramp for structural-folding with the following program: 80 to 60 °C at 5 min/°C, 60 to 10 °C at 75 min/°C, and finally holding at 10 °C (C1000 Thermal Cycler, Bio-Rad). The samples were then purified by gel filtration (Sephacryl S-400) to remove the excess DNA staple strands. Amicon Ultra-0.5 centrifugal filter devices (100 kDa) were used for the concentration of DNA scaffolds. The concentration of DNA scaffold was quantified by measuring the absorbance at 260 nm (Nanodrop, Thermo Fisher Scientific Inc.) using the determined extinction coefficient of DNA scaffold (1.2×10^8 M^{-1} cm^{-1}).[17]

2.2.2. Overexpression and Purification of ZS-XR and ZS-CA. The overexpression and purification of enzymes, ZS-XR (modular adaptor ZF-SNAP fused xylose reductase) and ZS-CA (modular adaptor ZF-SNAP fused carbonic anhydrase) were carried out as previously reported.[21,22]

2.2.3. Preparation of Benzylguanine (BG)-Modified Oligonucleotides (ODNs). A coupling reaction between amino modified oligonucleotides (ODNs) (100 μM) and succinimidyl derivative of SNAP-tag substrates (BG: 10 mM) was carried out in a 50 mM phosphate buffer (pH 8.0) for 24-h at ambient temperature. The BG-modified ODNs were purified by reversed-phase HPLC on a Cosmosil $5C_{18}$-MS II column (4.6 mm × 150 mm, elution with 100 mM triethylammonium acetate buffer (TEAA buffer), pH 7.0, linear gradient over 30 min from 5% to 60% acetonitrile at flow rate of 1.0 mL/min), and characterized by MALDI-TOF mass spectrometry (AXIMA-LNR, Shimadzu, HPA matrix).[23]

2.2.4. Preparation of the DNA Scaffold Assembled with ZS-XR or ZS-CA. DNA scaffolds were constructed either containing the binding sites (hairpin DNA) with BG modification for ZS-XR attachment or ZS-CA attachment. In a typical experiment, 10 nM DNA scaffold with three binding sites was incubated with 200 nM ZS-XR or ZS-CA in a binding buffer (pH 7.0) containing 40 mM Tris-HCl, 20 mM acetic acid, and 12.5 mM $MgCl_2$, 5 mM β-mercaptoethanol, 0.002% Tween20 and 1 μM $ZnCl_2$ at 4 °C for 1 h. After that, the mixture was purified by gel filtration (500 μL in volume of Toyopearl HW55F) in an Ultrafree-MC-DV column with a buffer (pH 7.0) containing 40 mM Tris-HCl, 20 mM acetic acid, and 12.5 mM $MgCl_2$ to remove the excess amount of unbound proteins. The concentration of DNA scaffold-protein complexes was quantified by measuring the absorbance at 260

https://doi.org/10.1021/acsami.4c18192
ACS Appl. Mater. Interfaces 2025, 17, 15775−15792

nm and calculated by using the determined extinction coefficient of DNA scaffold (1.2×10^8 M^{-1} cm^{-1}).[17]

2.3. AFM Imaging and Statistical Analysis. The characterization of DNA scaffolded enzymes by AFM was conducted as previously reported.[17] In brief, the sample was deposited on freshly cleaved mica (1.5 mm ϕ) surface and incubated for 5 min at ambient temperature, then washed three times with a buffer (pH 7.0) containing 40 mM Tris-HCl, 20 mM acetic acid, and 12.5 mM $MgCl_2$. Then the sample was scanned in a tapping mode using a fast-scanning AFM system (Nano Live Vision, RIBM Co. Ltd., Tsukuba, Japan) with a silicon nitride cantilever (Olympus BL-AC10DS-A2). At least three independent preparations of each sample were analyzed by AFM, and several images were acquired from different regions of the mica surface. The total number of DNA scaffolds corresponded to the well-formed structures observed under AFM. The binding of ZS-XR or ZS-CA was counted for only ZS-XR or ZS-CA bound to the perfectly folded DNA scaffold.

2.4. Quantification of Enzymes on the DNA Scaffold. The enzyme loading yield of ZS-XR or ZS-CA are quantitated by AFM images. The quantification process was conducted as previously reported.[17] The counting results of the assembled enzyme molecules on the DNA scaffold was shown in Supporting Information. DNA scaffold was constructed with three binding sites, the typical loading numbers of ZS-XR ($N_{ZS\text{-}XR}$) on each DNA scaffold were 2.54 molecules of monomer of ZS-XR; the typical loading numbers ZS-CA ($N_{ZS\text{-}CA}$) on each DNA scaffold were 2.55 molecules of monomer of ZS-CA.

2.5. Estimation of the Concentration of DNA-Scaffolded Enzyme. The concentration of DNA scaffold was quantitated by using a NanoDrop spectrophotometer (Thermo Fisher Scientific Inc.) at 260 nm and calculated by the determined extinction coefficient of DNA scaffold ($\varepsilon_{DNA\ scaffold} = 1.2 \times 10^8$ M^{-1} cm^{-1}).[17] The concentration of DNA-scaffolded enzyme was calculated as followed:

$$[\text{ZS-XR}]\ (\text{nM}) = N_{ZS\text{-}XR} \times \frac{A260}{\varepsilon_{DNA\ scaffold} \times l} \times 10^9$$

$$[\text{ZS-CA}]\ (\text{nM}) = N_{ZS\text{-}CA} \times \frac{A260}{\varepsilon_{DNA\ scaffold} \times l} \times 10^9$$

Where $N_{ZS\text{-}XR}$ or $N_{ZS\text{-}CA}$ is the loading numbers of ZS-XR or ZS-CA bound on the binding sites on the DNA scaffold by the statistical analysis of AFM images ($N_{ZS\text{-}XR} = 2.54$; $N_{ZS\text{-}CA} = 2.55$). A_{260} is the absorbance at 260 nm of the sample after purification, l is the path length (1 cm).

2.6. Enzyme Assays. *2.6.1. Enzyme Reactions for ZS-XR.* Catalytic activity of ZS-XR was analyzed according to the previously reported methods by measuring the changes of absorbance at 340 nm (25 °C) derived from the oxidation of NADH in an Infinite 200 PRO microplate reader (TECAN).[21] In a typical experiment, a reaction was started with an addition of NADH (300 μM) to a mixture of ZS-XR (25 nM monomer) and D-xylose (200 mM) in a buffer (pH 7.0) containing 40 mM Tris-HCl, 20 mM acetic acid, 12.5 mM $MgCl_2$, 100 mM NaCl, 1 μM $ZnCl_2$, 5 μM BSA and 0.002% Tween20. Enzyme activities were measured on the microplate (Greiner Microplate, 675801, UV-STAR Microplate, 96 well, Half area). The enzyme reaction conditions were specified in the captions of figures.

2.6.2. Measurement of Kinetic Parameters of ZS-XR in Free or Scaffolded Forms. The kinetic parameters of ZS-XR in free or DNA-scaffolded forms were measured for the substrate, D-xylose or *o*-chloroacetophenone. The enzyme reactions were performed by 25 nM free ZS-XR or scaffolded ZS-XR in a buffer (pH 7.0) containing of 500 μM NADH, 40 mM Tris-HCl, 20 mM acetic acid, 12.5 mM $MgCl_2$, 100 mM NaCl, 1 μM $ZnCl_2$, 5 μM BSA and 0.002% Tween20 in the presence of D-xylose or *o*-chloroacetophenone. The concentrations of D-xylose were varied from 50 mM to 500 mM, and the concentrations of *o*-chloroacetophenone were varied from 500 μM to 5 mM. The enzyme reactions of *o*-chloroacetophenone were conducted with 5% ethanol. The values of K_m and V_{max} were obtained by the Lineweaver−Burk plotting. The value of k_{cat} was calculated from the value of V_{max} divided by the concentration of enzyme.

2.6.3. Enzyme Reactions for ZS-CA. Commercial *p*-nitrophenyl acetate (*p*-NPA), *p*-nitrophenyl butyrate (*p*-NPB) and *p*-nitrophenyl valerate (*p*-NPV) were first dissolved in 100% acetone to the concentration of 10 mM. The final concentration of substrate in the reaction was set to 0.1 mM in the presence of 5% acetone. The substrate was prepared freshly prior to the reaction. The reaction mixture was composed of a buffer (pH 7.6) containing 50 mM HEPES, 12.5 mM $MgCl_2$, 5% acetone, 1 μM $ZnCl_2$ and 0.002% Tween20 with 0.1 mM substrate. In a typical reaction, the reaction was started by the addition of 5 μL of substrate in 100% acetone to 100 μL reaction. Due to the low reactivity of ZS-CA toward the substrates causing the difficulty in observation at 348 nm (isosbestic point of *p*-nitrophenol and *p*-nitrophenolate), the reaction was monitored at a maximum of absorbance at 400 nm (at pH 7.6) with extinction coefficients of 1.28×10^4 M^{-1} cm^{-1}.[22] Enzyme activities were measured on the microplate (Greiner Microplate, 675801, UV-STAR Microplate, 96 well, Half area) at 25 °C. The enzyme reaction conditions were specified in the captions of figures.

2.7. Calculation of the Thermodynamic Quantities of Hydration for Solutes (Substrates). All-atom models and molecular models were adopted for the substrates and for water, respectively. The three-dimensional (3D) structures of the substrates were modeled using Discovery Studio (version 3.1, Accelrys Inc.). The general AMBER force field (GAFF)[24] was employed, and the AM1-BCC method[25,26] was applied to the determination of the set of atomic charges using the antechamber module in the AMBER 2018 program package.[27] The thermodynamic quantities of hydration of the substrates employed in our experiments were calculated using a hybrid[18] of the angle-dependent integral equation theory[28−31] combined with the morphometric approach[32] and the 3D reference interaction site model (3D-RISM) theory.[33,34] This hybrid method gives very accurate values of the hydration free energy for solutes.[18] Comparison between theoretically calculated and experimentally measured values for hydration free energy of a solute is shown in Table 1. The hydration free energy μ,

Table 1. Comparison between Theoretically Calculated and Experimentally Measured Values for the Hydration Free Energy of a Solute

substrate	μ(kcal/mol); theoretical	μ (kcal/mol); experimental
D-xylose	−16.7	−15.0
4-NBA	−8.49	−8.83 (4-hydroxybenzaldehyde)
o-CAP	−3.02	−4.58 (acetophenone)
water molecule	−6.34	−6.30

https://doi.org/10.1021/acsami.4c18192
ACS Appl. Mater. Interfaces 2025, 17, 15775−15792

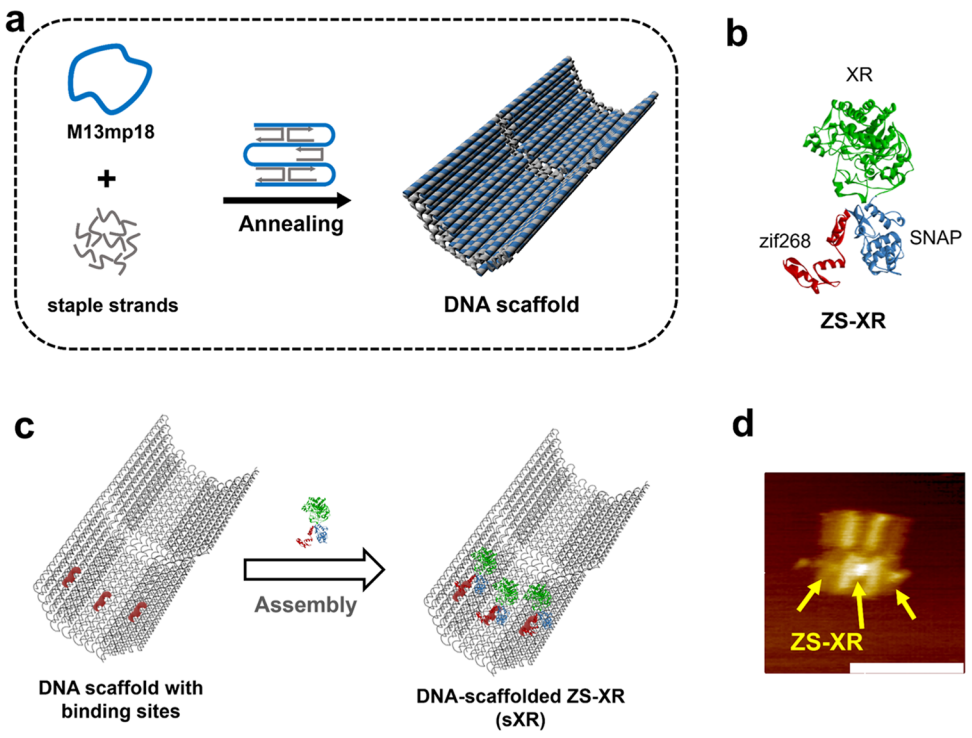

Figure 1. Assembly of enzymes on the DNA scaffold. (a) Construction of DNA scaffold by annealing the long single-stranded DNA (M13mp18) with DNA staple strands.[17] (b) A molecular model representing ZS-XR (modular adaptor ZF-SNAP fused xylulose reductase).[21] (c) An illustration representing ZS-XR assembled on the DNA scaffold (sXR). The scaffold was constructed with three enzyme binding sites. (d) A typical AFM image of ZS-XR assembled on the DNA scaffold. Scale bar: 100 nm. The arrows indicated the bound ZS-XR.

substrate-water electrostatic interaction energy ε_{ES} normalized by the water-accessible surface area of the substrate A, and hydration entropy S calculated are collected in Table 2. The Table includes Log P, a measure of the hydrophilicity or hydrophobicity of the substrate usually used in the chemical research community.

2.8. Code Availability. In the procedure of calculating the hydration free energy (μ), energy (ε), and entropy (S) of a solute,[18] the hydration of the solute is decomposed into Processes 1 and 2:

Process 1: Creation of a cavity matching atomistic, geometric characteristics of the solute. This process is the hydrophobic hydration.

Process 2 comprises Processes 2-vdW and 2-ES.

Process 2-vdW: Incorporation of solute-water van der Waals (vdW) interaction.

Process 2-ES: Incorporation of solute-water electrostatic (ES) interaction.

The four coefficients in the morphometric forms required in Process 1 are given in an earlier publication by the group of Kinoshita,[35] and the four geometric measures of the solute can be evaluated using a computer code AlphaMol recently made available by another group[36] as an OpenSource software on GitHub (https://github.com/pkoehl/AlphaMol). By applying the computer code of the 3D-RISM theory[33,34] in the AmberTools program package (https://ambermd.org/AmberTools.php) to Process 2, one can finish the calculations for Processes 1 and 2 and obtain the numerical values of μ, ε, and S. The solute-water electrostatic interaction energy ε_{ES} can be calculated using the computer code of the 3D-RISM theory.

3. RESULTS AND DISCUSSION

3.1. Enzyme Assembly on the DNA Scaffold. A three-dimensional hexagonal prism DNA scaffold in its fully open state was constructed as previously reported.[17] This DNA scaffold consisted of two boat shapes covalently attached at the back by single-stranded scaffold hinges with the dimensions of 70 nm × 45 nm × 17.5 nm (Figure 1a, Figures S1 and S2). The modular adaptor was used to specifically assemble enzymes onto the DNA scaffold with high loading yields.[21,23,37−39] Xylose reductase (XR), an enzyme derived from D-xylose metabolic pathways, was genetically fused to the modular adaptor ZF-SNAP (ZS) to yield ZS-XR (Figure 1b).[21] In this construct, the zif268 bound to the specific DNA sequence on the DNA scaffold, while the SNAP-tag reacted with benzylguanine (BG) incorporated in the DNA sequence to form a covalent bond (Figure S3a).[21] ZS-XR was assembled on the DNA scaffold with three BG-modified binding sites (Figure 1c, Figure S3a−S3c, and Table S1). The enzyme-assembled DNA scaffolds were purified by gel filtration to remove the unbound ZS-XR. The enzyme loading yield on the DNA scaffold was estimated from the AFM images (Figures 1d and S4) as previously reported.[17] On average, ZS-XR was assembled with 2.5 molecules of monomer on each DNA scaffold (Table S2). In the following, DNA-scaffolded ZS-XR would be referred to as "sXR." The distance between the enzyme and DNA surfaces varied widely, ranging from 0 to 5.5 nm (Figure S3b).

3.2. Reactions of Hydrophilic and Hydrophobic Substrates by Xylose Reductase. Various substrates have been studied for the catalytic reaction of XR. In order to verify the generality of the catalytic enhancement of XR on the DNA scaffold, enzyme reactions were carried out for free ZS-XR or

https://doi.org/10.1021/acsami.4c18192
ACS Appl. Mater. Interfaces 2025, 17, 15775−15792

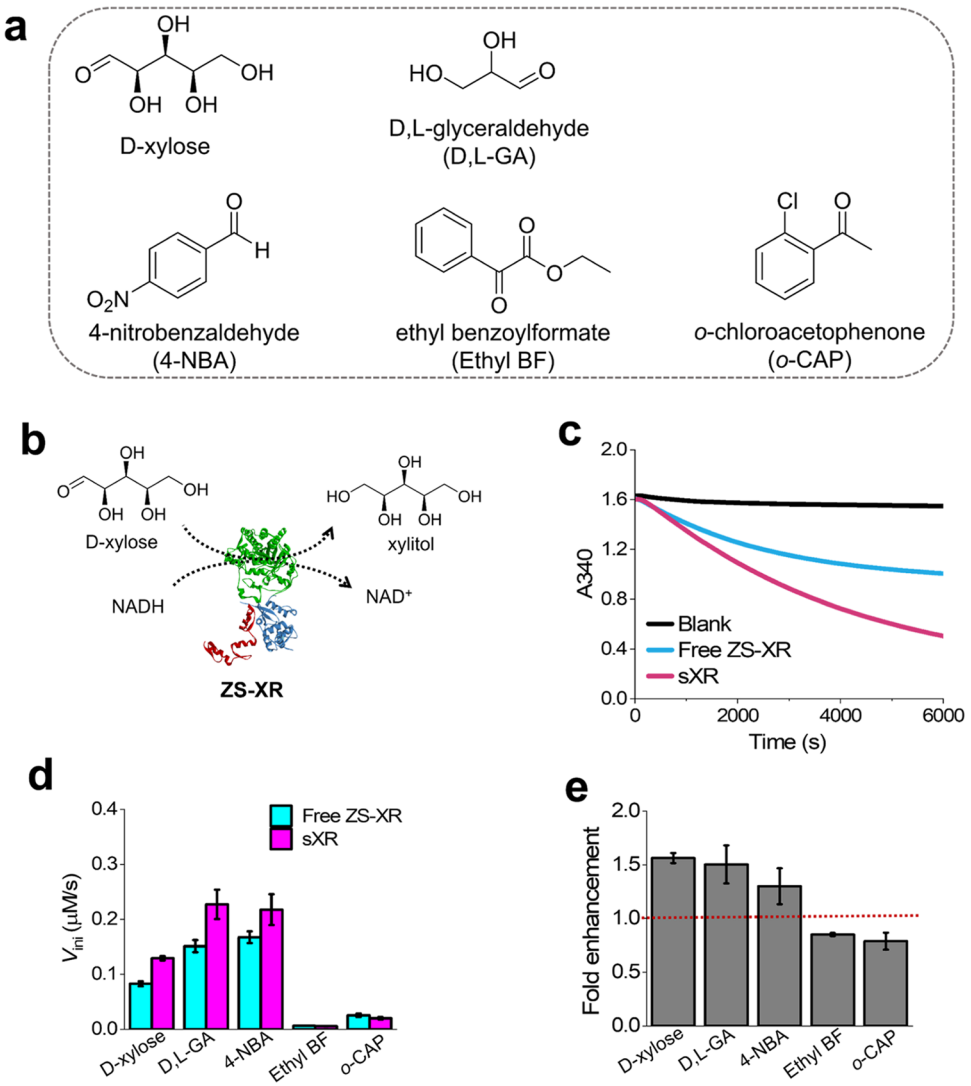

Figure 2. Reactions of hydrophilic and hydrophobic substrates by xylose reductase. (a) Substrates used for xylose reductase reactions. (b) The Scheme of ZS-XR-catalyzed reaction that converts D-xylose to xylitol with a consumption of NADH. (c) Time course profiles of the absorbance at 340 nm (A340) of the enzyme reaction of free ZS-XR or sXR. (d) V_{ini} of the enzyme reaction for 25 nM free ZS-XR or sXR with each of the substrates tested. (e) FE by sXR against each of the substrates tested. The enzyme reactions of XR were carried out with 25 nM free ZS-XR or sXR in the presence of 50 mM D-xylose, 15 mM D,L-GA, 1 mM 4-NBA, 2 mM Ethyl BF, or 2 mM *o*-CAP.

sXR using a variety of substrates, D-xylose,[40] D,L-glyceraldehyde (D,L-GA),[41] 4-nitrobenzaldehyde (4-NBA),[42] ethyl benzoylformate (Ethyl BF),[43] and *o*-chloroacetophenone (*o*-CAP)[44] (Figure 2a). As we will show in a later section, the classification of the hydrophilicity or hydrophobicity of a given substrate is an important step toward the elucidation of our experimental observations and needs to be made based on the results from our accurate statistical mechanics analyses. Here, for convenience, we roughly describe the property of a substrate in terms of Log P, a conventional measure of the hydrophilicity or hydrophobicity. As shown in Table 2, D-xylose and D,L-GA are hydrophilic (Log P < 0) since they possess hydroxyl groups whereas 4-NBA, Ethyl BF, and *o*-CAP are hydrophobic (Log P > 0) due to the presence of benzene rings (Figure 2a). The enzyme reaction schemes for XR with different substrates are shown in Figures 2a and S5. XR converted D-xylose, D,L-GA, 4-NBA, Ethyl BF, or *o*-CAP to xylitol, glycerol, 4-nitrobenzyl alcohol, ethyl (*R*)-mandelate, or 1-(*o*-chlorophenyl)-ethanol, respectively. As shown in our previous study, assembling enzymes on a large, negatively charged DNA scaffold can reduce enzyme adsorption on the surface of reaction vessel, resulting in higher enzyme activity compared to free enzymes.[17] To evaluate this possible effect, enzyme reactions were carried out for ZS-XR by increasing the enzyme concentration from 5 to 25 nM. For free ZS-XR, we observed that the reaction rate was almost linearly dependent on the enzyme concentration above 20 nM (Figure S6). Therefore, at an enzyme concentration of 25 nM, the effect of enzyme adsorption to the surface of reaction vessel could be neglected. In this study, the enzyme reactions were carried out at an enzyme concentration of 25 nM. Time course of the reactions for different substrate was analyzed by spectrophotometric monitoring of NADH consumption at 340 nm (Figures 2c and S7). The initial reaction velocity (V_{ini}) of enzyme reactions were calculated by using the time course of absorbance at 340 nm (Figure 2d).

The catalytic fold enhancement (FE) is defined as "V_{ini} for an enzyme loaded on the DNA scaffold divided by V_{ini} for a free enzyme" to evaluate the catalytic enhancement of the enzyme assembled on the DNA scaffold. The FEs for sXR with

https://doi.org/10.1021/acsami.4c18192
ACS Appl. Mater. Interfaces 2025, 17, 15775−15792

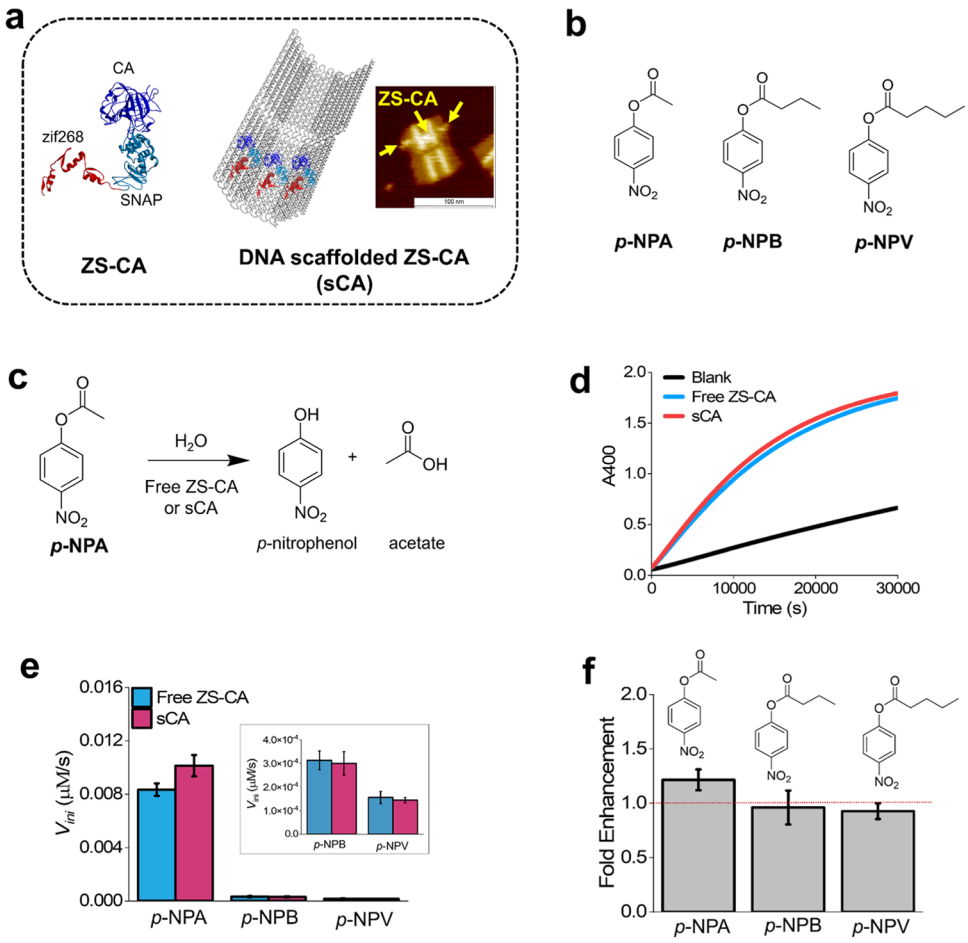

Figure 3. Reactions of hydrophobic substrates by carbonic anhydrase. (a) Left: an illustration of ZS-CA assembled on the DNA scaffold; right: a typical AFM image of ZS-CA assembled on the DNA scaffold (sCA). Scale bar: 100 nm. (b) Structures of *p*-NPA, *p*-NPB, and *p*-NPV. (c) The CA-catalyzed hydrolysis of the substrate *p*-NPA resulted in the production of *p*-nitrophenol and acetate. (d) Time course of the absorbance at 400 nm (A400) of the enzyme reaction for free ZS-CA or sCA with *p*-NPA. (e) V_{ini} of the enzyme reaction for ZS-CA or sCA with each of the substrates tested. (f) FE of the sCA reaction to each of the substrates tested. FE of sCA represents "V_{ini} for sCA divided by V_{ini} for free ZS-CA". Enzyme reactions for CA were carried out at 25 nM free ZS-CA or sCA with 100 μM *p*-NPA, *p*-NPB, or *p*-NPV in a buffer (pH 7.6) containing 50 mM HEPES, 12.5 mM $MgCl_2$, and 5% acetone.

D-xylose, D,L-GA, and 4-NBA decreased to 1.6, 1.5, and 1.3, respectively. Interestingly, the FEs for sXR with Ethyl BF and *o*-CAP decreased to 0.85 and 0.79, respectively (Figure 2e). V_{ini} for sXR with Ethyl BF and *o*-CAP was slower than that for free ZS-XR, resulting in FEs less than 1 (Figure 2d,e). The FE follows the order, D-xylose > D,L-GA > 4-NBA>*o*-CAP > Ethyl BF, which is somewhat correlated with Log P.

Detailed kinetic analyses were performed for the enzyme reactions at 25 nM free ZS-XR or sXR (Figures S8−S13, Tables S3 and S4). The Michaelis−Menten constant (K_m) varies little between free ZS-XR (130.2 mM) and sXR (136.2 mM) for D-xylose. On the other hand, sXR showed larger turnover number (k_{cat}) than free ZS-XR for D-xylose. The values of k_{cat}/K_m of free ZS-XR and sXR for D-xylose were 0.094 and 0.126 mM^{-1} s^{-1}, respectively, indicating the accelerated reaction of the enzyme assembled on the DNA scaffold for xylose by a factor of 1.3 (Table S3). For *o*-CAP, the K_m values of free ZS-XR and sXR were 2.14 and 4.95 mM, respectively. The values of k_{cat}/K_m of free ZS-XR and sXR for *o*-CAP were 0.95 and 0.66 mM^{-1} s^{-1}, respectively, indicating the decelerated reaction of the enzyme assembled on the DNA scaffold for *o*-CAP by a factor of 0.79 (Table S4). These results manifest that the FE described above well represents the differences in k_{cat} and K_m for free ZS-XR and sXR.

3.3. Reactions of Hydrophobic Substrates by Carbonic Anhydrase. To further test the substrate-dependent effect of the DNA scaffold on the enzyme reaction, enzyme reactions for CA were performed with several substrates. CA was genetically fused to the modular adaptor ZF-SNAP to obtain the construct ZS-CA.[22,45] The DNA scaffolds were constructed with three BG-modified binding sites for the attachment of ZS-CA (Figures 3a and S3). The enzyme loading yield of ZS-CA on the DNA scaffold was quantified using AFM images (Figure S14, and Table S5) as described for ZS-XR. On average, ZS-CA was assembled with 2.6 molecules of monomer on each DNA scaffold (Table S5).

The hydrolysis reactions of *p*-nitrophenyl acetate (*p*-NPA), *p*-nitrophenyl butyrate (*p*-NPB), or *p*-nitrophenyl valerate (*p*-NPV) catalyzed by free ZS-CA and ZS-CA assembled on the DNA scaffold (sCA) at an enzyme concentration of 25 nM were measured by monitoring the production of *p*-nitrophenol spectrophotometrically at 400 nm (A400), where *p*-nitrophenol showed the maximum absorbance value (Figure 3b,c, Figure S15, S16). The V_{ini} values of free ZS-CA and sCA were calculated and shown in Figure 3e. FE, representing "V_{ini} for

https://doi.org/10.1021/acsami.4c18192
ACS Appl. Mater. Interfaces 2025, 17, 15775−15792

sCA divided by V_{ini} for free ZS-CA," was used to evaluate the catalytic enhancement of sCA. The FEs for sCA with *p*-NPA and *p*-NPB decreased to 1.2 and 0.9, respectively. The FE for the sCA with *p*-NPV was 0.9. The FE values for the hydrophobic substrates *p*-NPA, *p*-NPB and *p*-NPV were not significantly different from those observed for the reactions of the hydrophobic substrates Ethyl BF and *o*-CAP with XR. The Log P values of *p*-NPA, *p*-NPB, and *p*-NPV were 1.56, 2.47, and 2.93, respectively, indicating increased hydrophobicity of the CA substrates (Table 2). This suggests that the hydrophobicity of the substrate affects the enzyme reaction on the DNA scaffold, which was further investigated and discussed in the following sections.

3.4. Statistical Mechanics Analyses of the Hydration Properties of Substrates. The hydration properties of substrates can provide clues to the modulation of enzyme reactions. We calculated the hydration free energy μ and its energetic and entropic components, ε and S ($\mu = \varepsilon - TS$ where T is the absolute temperature), using an accurate statistical mechanics theory developed by Kinoshita and co-workers which is referred to as "cHybrid"[18] (The decomposition of μ into ε and S is performed under the isochoric condition: See Note S1). cHybrid is a hybrid of the angle-dependent integral equation theory[28−31] combined with the morphometric approach[32] and the three-dimensional (3D) reference interaction site model (3D-RISM) theory.[33,34] The 3D structure of a solute is taken into account at the atomic level and a molecular model is employed for water. cHybrid gives very accurate values of the hydration free energy for solutes with various sizes including small organic molecules, peptides, and proteins.[18] For the small organic molecules, the theoretical values are in very good agreement with the experimentally measured values. For the peptides and proteins, there are no experimentally measured values, but the theoretical values are very close to the values calculated by a new type of all-atom MD simulation with explicit water which is much more efficient than the usual MD simulation.[18]

In this study, the 3D structures of the substrates were modeled using Discovery Studio (version 3.1, Accelrys Inc.). The general AMBER force field (GAFF)[24] was employed, and the AM1-BCC method[25,26] was applied to the determination of the set of atomic charges using the antechamber module in the AMBER 2018 program package.[27]

Table 1 is designated to compare theoretically calculated and experimentally measured values for the hydration free energy of a solute. In the literature, we could find experimental data only for D-xylose pyranose[46] and a water molecule.[47] As can be seen from Table 1, the agreement for the water molecule is almost perfect and that for D-xylose pyranose is quite good. The reasons for the small discrepancy for D-xylose pyranose may be as follows: Its 3D structure used in the calculation is that in vacuum; the change in the 3D structure upon the insertion into water and the structural fluctuation in water are both neglected; and the force field is not free of the uncertainty. The experimentally measured value for 4-hydroxybenzaldehyde is −8.83 kcal/mol.[48] Replacing the "OH" group in 4-hydroxybenzaldehyde with "NO_2" results in 4-nitrobenzaldehyde. Since "NO_2" is less hydrophilic than "OH", the μ of 4-nitrobenzaldehyde should be higher (i.e., shift in a positive direction) than −8.83 kcal/mol: It is −8.49 kcal/mol that is reasonable. The experimentally measured value for acetophenone is −4.58 kcal/mol.[48] Replacing "H" in acetophenone to "Cl" yields *o*-chloroacetophenone. Since "Cl" is much larger than "H", the μ of *o*-chloroacetophenone should be much higher than −4.58 kcal/mol: It is −3.02 kcal/mol that is reasonable. Thus, it can be concluded that the theoretically calculated values are in good agreement with the experimentally measured values.

There are two principal quantities of a substrate that affect μ: the excluded volume (EV) and the energetic affinity for water. Here, EV is the volume of space that is inaccessible to the centers of water molecules in the system. The hydration entropy, $S < 0$, is primarily dependent on the EV of the substrate. The larger the EV, the higher $|S|$ is. The energetic affinity of the substrate for water increases as the proportion of charged and polar groups on the water-accessible surface (WAS) of the substrate increases. Even when the WAS of the substrate is predominantly nonpolar, $|\varepsilon|$ ($\varepsilon < 0$ is the hydration energy) increases as the water-accessible surface area (WASA) of the substrate increases owing to the lowered substrate-water van der Waals interaction energy. It follows that ε is not a good measure of the energetic affinity of the substrate for water. The most relevant measure is ε_{ES}/A where $\varepsilon_{ES} < 0$ and A denote the substrate-water electrostatic interaction energy and WASA, respectively. Even when the proportion of charged and polar groups on the WAS of the substrate is smaller, $|\varepsilon_{ES}|$ becomes higher when A is substantially larger. Thus, it is important to normalize ε_{ES} by A.

The values of μ, ε_{ES}/A, and TS calculated are collected in Table 2 (T is the absolute temperature). The Table includes

Table 2. Four Representative Parameters Calculated for the Substrates of Xylose Reductase Or Carbonic Anhydrase[a]

	Log P	μ (kcal/mol)	ε_{ES}/A [kcal/(mol nm^2)]	$-TS$ (kcal/mol)
D-xylose[b]	−1.84	−16.7	−5.73	34.88
D,L-GA	−1.63	−9.75	−4.71	24.56
4-NBA	1.3	−8.49	−2.83	37.22
ethyl BF	1.73	−4.41	−2.56	49.44
o-CAP	1.9	−3.02	−2.02	40.06
p-NPA	1.56	−6.71	−2.61	45.49
p-NPB	2.47	−3.28	−2.20	56.30
p-NPV	2.93	−1.58	−1.95	61.32

[a]The parameters of D-xylose were calculated using the structure of D-xylopyranose. [b]The parameters of D-xylose were computed and calculated by using the structure of D-xylopyranose. T is the absolute temperature.

Log P, a measure of the hydrophilicity or hydrophobicity of the substrate usually used in the chemical research community. In terms of the Log P values, the substrates tested in this study can be categorized as hydrophilic (D-xylose and D,L-GA) and hydrophobic (4-NBA, Ethyl BF, *o*-CAP, *p*-NPA, *p*-NPB, and *p*-NPV) substrates (Figure 4a). However, we found that this Log P-based categorization was not suitable for describing the experimentally obtained FE values, as evidenced by the result that the FE of 4-NBA was similar to that of D-xylose and D,L-GA (Figure 4a), despite the large difference in the Log P values.

The FE of 25 nM sXR or sCA is plotted against μ, Log P, ε_{ES}/A, and $-TS$ calculated for the substrates in Figure 4b−d. In Figure 4b, the vertical dot line indicates the experimentally measured hydration free energy of a water molecule, $\mu_{exp} = -6.30$ kcal/mol.[47] The hydration free energy of a water molecule calculated by our statistical mechanics theory[18] is

https://doi.org/10.1021/acsami.4c18192
ACS Appl. Mater. Interfaces 2025, 17, 15775−15792

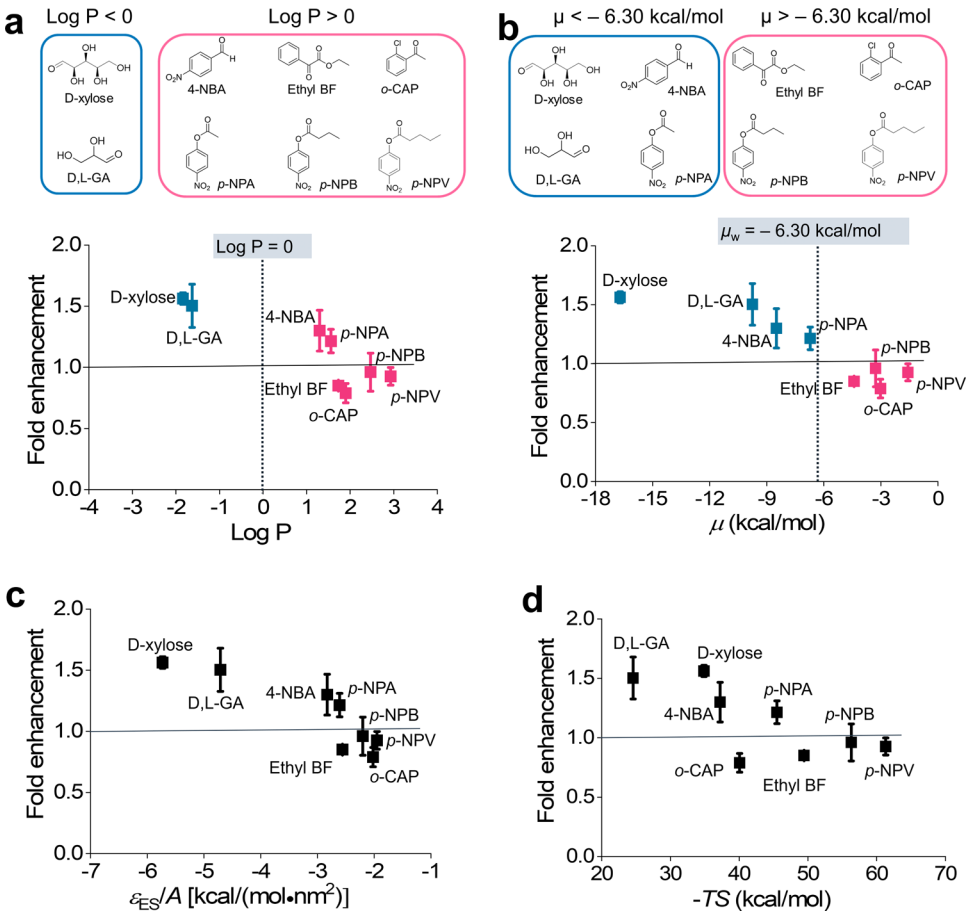

Figure 4. FE by 25 nM sXR or sCA plotted against four representative parameters calculated for the substrates. (a) Top: categorization of the substrates in terms of Log P; bottom: plot of FE against Log P of the substrates. (b) Top: categorization of the substrates in terms of the hydration free energy, μ; bottom: plot of FE against μ of the substrates. (c) Plot of FE against ε_{ES}/A of the substrates. (d) Plot of FE against $-TS$ of the substrates. The dotted lines in a,b denote Log P = 0 and μ = −6.30 kcal/mol, respectively.

−6.34 kcal/mol, which is in good agreement with the experimental value. The quantitative reliability of the μ values calculated for the substrates is corroborated in Table 1 and its associated discussion. Substrates with $\mu < \mu_{exp}$ behave as hydrophilic solutes (D-xylose, D,L-GA, 4-NBA, and *p*-NPA), whereas those with $\mu > \mu_{exp}$ behave as hydrophobic solutes (Ethyl BF, *o*-CAP, *p*-NPB, and *p*-NPV) (Figure 4b). Water favors a substrate with $\mu < \mu_{exp}$ more than a water molecule. Likewise, water favors a water molecule more than a substrate with $\mu > \mu_{exp}$. Importantly, the experimentally obtained FE is larger than 1 for the hydrophilic substrates, whereas it is smaller than 1 for the hydrophobic substrates (Figure 4b).

We calculated the correlation coefficients for the FE and the four quantities μ, Log P, ε_{ES}/A, and $-TS$. The values obtained for μ, Log P, ε_{ES}/A, and $-TS$ were −0.902, −0.869, −0.883, and −0.717, respectively. The negative sign indicates that FE decreases with an increase in any of the four quantities. The FE is best correlated with μ. Furthermore, the correlation between FE and ε_{ES}/A is stronger than that between FE and $-TS$. The hydration free energy μ is the excess chemical potential of a solute and the free-energy change upon transfer of the solute with a fixed structure from vacuum to water. On the other hand, P is the ratio of the solute concentration in the organic solvent, usually octanol, to that in water (the organic solvent is in equilibrium with the water). It is difficult to distinguish hydrophilic substrates from hydrophobic ones in terms of Log P. If the distinction is made by the vertical dot line (Log P = 0) in Figure 4a, the FE becomes unreasonably larger than 1 for the two substrates 4-NBA and *p*-NPA, which are classified as hydrophobic substrates. Therefore, μ is more suitable than Log P as a measure of the hydrophilicity or hydrophobicity of the substrate, despite the common use of Log P in the chemical research community. Because FE correlates better with ε_{ES}/A than with $-TS$ (Figure 4c,d), FE can be discussed in terms of the energetic affinity of the substrate for water as the key factor. Our experimental results indicate that FE > 1 for substrates with relatively higher energetic affinity (D-xylose, D,L-GA, 4-NBA, and *p*-NPA) and FE < 1 for substrates with a relatively lower energetic affinity (Ethyl BF, *o*-CAP, *p*-NPB, and *p*-NPV). In a prevailing view, solutes with μ<0 and with μ>0 are considered hydrophilic and hydrophobic, respectively. This view is suited to a discussion on the solubility of the solute in water. However, in the present case where we wish to know which of the solute concentrations in the high-density water layer and in bulk water is higher, solutes with $\mu<\mu_{exp}$ and with $\mu > \mu_{exp}$ should be considered hydrophilic and hydrophobic, respectively. This is our important finding.

3.5. Structure and Properties of the High-Density Water Layer on the DNA Scaffold Surface. The DNA strand has an array of negatively charged phosphate groups that are exposed to water. Near such a group, a water molecule turns its dipole moment toward the group, and water

https://doi.org/10.1021/acsami.4c18192
ACS Appl. Mater. Interfaces 2025, 17, 15775−15792

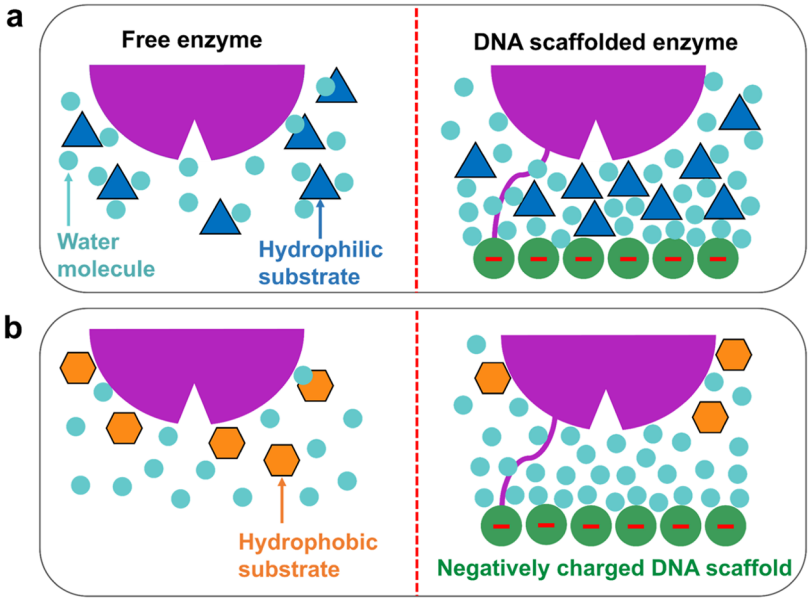

Figure 5. A diagram illustrating the effect of high-density water layer near the DNA scaffold surface on enzyme reactions. It shows a snapshot in which the active site of the enzyme is sufficiently close to the DNA scaffold surface. (a) The high-density water layer near the DNA scaffold surface increases the concentration of a hydrophilic substrate within the layer, leading to an acceleration of the enzyme reaction. (b) The high-density water layer near the DNA scaffold surface decreases the concentration of a hydrophobic substrate within the layer, resulting in a slowing of the enzyme reaction.

molecules are strongly attracted to the group due to the group-dipole moment electrostatic attractive interaction, leading to the formation of a layer near the group in which the water density is much higher than that in bulk water (case 1). It is known that a phosphate group is strongly hydrated.[49] This is consistent with the explanation given above. Here, we consider a case when a negatively charged group is immersed in electrolyte solution. In such a case, cations are strongly attracted to the group due to the group-cation electrostatic attractive interaction, with the result that the concentration of cations near the group becomes much higher than that in the bulk solution (case 2). We note that case 1 as well as case 2 can readily be understood from an electrostatic point of view.

The water layer characterized as in case 1 is not formed near the groups other than the phosphate groups, but the average density of water near the DNA strand becomes significantly higher than the density of bulk water. In fact, it has been shown by an all-atom molecular dynamics (MD) simulation with explicit water using a reliable force field[50] that the water density near the DNA strand is, on the average, twice higher than that in bulk water. Of course, the water densities near phosphate groups are even much higher. The DNA duplexes are highly packed in the DNA scaffold used in our experimental study. As a result, the water densities near the phosphate groups become quite high. To the best of our knowledge, there is no data based on a reliable experimental technique, which manifests the formation of a high-density water layer near the DNA scaffold surface. However, the result from the aforementioned MD simulation should be as convincing as an experimental result.

The charge density of a surface is a qualitatively good measure of the average density of water near the surface: As the surface charge density increases, the average density of water near the surface becomes higher.[51,52] The surface charge densities of B-DNA[53] and the DNA origami[54] (the DNA scaffold) were estimated to be ~ -16 and ~ -21 $\mu C/cm^2$, respectively (see Note S2 for a detailed explanation). Zhao et al.[16] also pointed out the high surface charge density of the DNA scaffold. The structure of water near a uniform, almost flat surface with a charge density of ~ -18 $\mu C/cm^2$ was analyzed using the angle-dependent integral equation theory (ADIET), a theory based on statistical mechanics for molecular liquids.[51] The analysis showed the following: The high surface charge density leads to the formation of a surface-induced layer of water in which the number density of water molecules is much higher than that in bulk water; but the thickness of this high-density layer of water is as small as ~1 nm, only 3−4 times larger than the diameter of a water molecule, 0.28 nm (see Note S3 for a more detailed discussion). Although the quantitative aspects of the calculated result for the density structure depend somewhat on the surface and water models used and the details of the theory,[51,52] it is definite that a high-density layer of water is formed near a surface whose charge density is significantly high, as in the cases of B-DNA and the DNA scaffold.

In Note S4, we remark that the following has been corroborated by not only elaborate statistical mechanics theories but also an all-atom MD simulation with explicit water using a reliable force field: A water molecule near an uncharged metal surface generating a positive electric field turns its dipole moment against the surface, and water molecules are attracted to the surface by the surface-dipole moment electrostatic attractive interaction, leading to the formation of a high-density layer of water near the surface. In conclusion, a high-density layer of water is formed near a surface with a high surface charge density or generating a strong electric field, regardless of its sign, negative or positive.

When enzymes are assembled on the DNA scaffold by binding the enzyme-fused modular adaptor[55] to a specific DNA duplex, the distance between the enzyme and the DNA scaffold surface fluctuates widely, ranging from 0 to 5.5 nm, due to the flexibility of the binding sites (hairpin DNA) and

https://doi.org/10.1021/acsami.4c18192
ACS Appl. Mater. Interfaces 2025, 17, 15775−15792

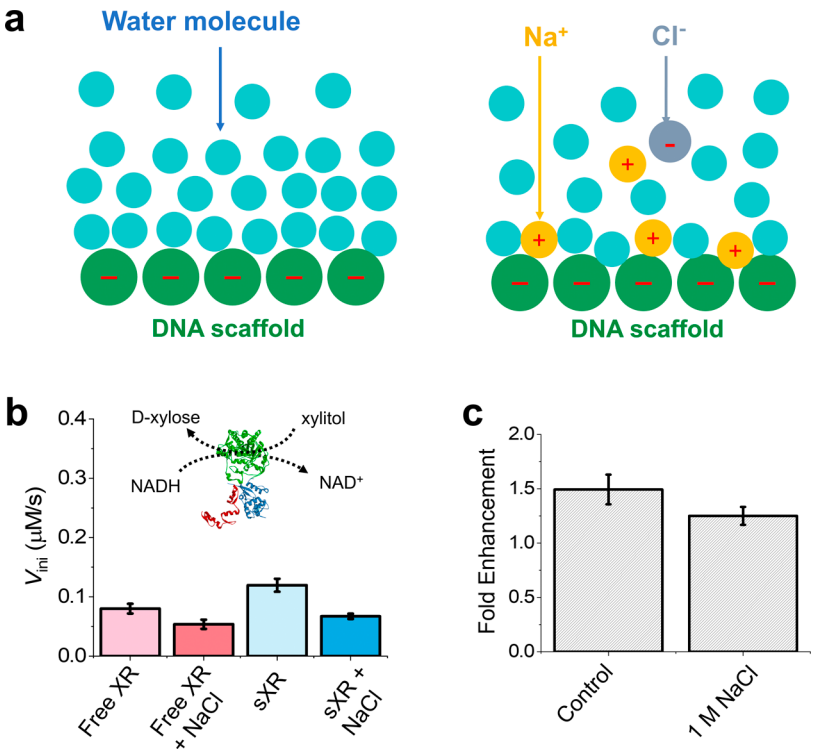

Figure 6. Effect of the salt on xylose reductase enzyme reactions of on DNA scaffold. (a) A diagram showing that the high-density water layer on the DNA scaffold surface is deformed in the presence of cations such as Na^+. (b) V_{ini} of the enzyme reaction for free ZS-XR or sXR in the absence or presence of 1 M NaCl. D-xylose was used as substrate. (c) FE of sXR reactions in the absence (control) and presence of 1 M NaCl. FE of sXR represents "V_{ini} for sXR divided by V_{ini} for free ZS-XR". Enzyme reactions were conducted for 25 nM free ZS-XR or 25 nM sXR with 50 mM D-xylose.

the linker region of the modular adaptor (Figure S3b). When the distance is short enough to bring the active site of the enzyme sufficiently close to the DNA surface, the enzymatic reaction proceeds under the influence of a high-density layer of water molecules, leading to a reaction velocity which is different from that in the vicinity of a free enzyme. This difference may play an essential role in the increased or decreased enzymatic reaction velocity observed in this study.

The local concentration (i.e., the concentration near a surface or within the space confined between two surfaces) of a substrate is determined by the interplay of energetic and entropic effects. Energetically, the local concentration of a substrate is closely related to the number density of water molecules in it (see 3.7 for discussion). Here we hypothesize the following: the concentration of a substrate with a high energetic affinity for water is higher near the enzyme part sufficiently close to the DNA surface than near a free enzyme surface, leading to a higher reaction velocity of the enzyme in the bulk solution (Figure 5a); however, the opposite is true for a substrate with a low energetic affinity for water, leading to a lower velocity of the enzyme reaction (Figure 5b).

3.6. Effect of the Salt on Xylose Reductase Enzyme Reactions of on the DNA Scaffold. The substrate concentration within the space confined between the enzyme and DNA surfaces (Figure 5a) can vary depending on the physicochemical properties of the substrate. As the next experimental test, a high concentration of cations, Na^+, was added to the aqueous solution to screen the negative charge of the phosphate group of DNA and to deform the high-density water layer (Figure 6a). The enzymatic reaction of 25 nM ZS-XR or sXR with D-xylose was analyzed by monitoring the consumption of NADH spectrophotometrically at 340 nm (Figure S17). The V_{ini} for both free ZS-XR and sXR was reduced in the presence of 1 M NaCl (Figure 6b). For the reaction of ZS-XR and D-xylose, FE was greater than 1 regardless of the salt addition (Figure 6c).

At 1 M NaCl, the values of V_{ini} for free ZS-XR and sXR were reduced to ~67 and ~56% of those in the absence of NaCl, respectively. The FE decreased from 1.5 to 1.2 in the presence of 1 M NaCl (Figure 6c). The reduction of V_{ini} for free ZS-XR can be explained as follows: A substrate with a high affinity for water, such as D-xylose, prefers to be hydrated in bulk water rather than coming in contact with the free enzyme, and this effect is enhanced by the addition of salt as discussed later (see Subsection 3.1).

The reduction in V_{ini} is more evident for sXR. The negative charges on the DNA surface were screened by the cation Na^+. Through this screening effect, the number density of water molecules within the surface-induced layer near the DNA nanostructure was reduced, and the enrichment of the D-xylose concentration within the layer was also reduced. The V_{ini} for sXR is higher than that for free ZS-XR because the screening is not complete, and the average number density of water molecules within the layer is still higher than that in the bulk. The reduced FE supported the hypothesis that surface-induced high-density water, which could be deformed by cations, was responsible for the FEt.

The screening effect by Na^+ is more reflected in V_{ini} than in FE. This is because not only V_{ini} for sXR but also V_{ini} for free ZS-XR is decreased by the NaCl addition and FE is affected by the decrease in V_{ini} for free ZS-XR as well. We can evaluate the screening effect by comparing the values of V_{ini} for sXR and

https://doi.org/10.1021/acsami.4c18192
ACS Appl. Mater. Interfaces 2025, 17, 15775−15792

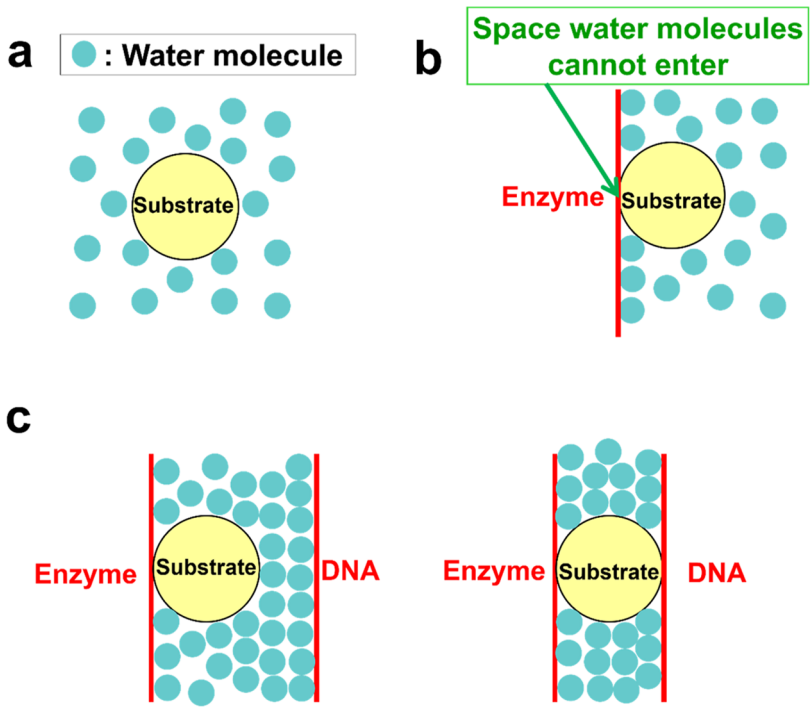

Figure 7. A substrate in (a) bulk water, in (b) the vicinity of a free enzyme, or in (c) a narrow domain confined between the enzyme and DNA surfaces (or in the vicinity of an enzyme close to the DNA surface). In the case of (c), the surface separation is variable. Within (c), when the surface separation is sufficiently small, the number density of water molecules near the enzyme is much higher than that near a free enzyme, owing to the effect of the high density layer of water molecules near the DNA surface.

sXR-NaCl in Figure 6b. V_{ini} for sXR-NaCl is slower, which is definite considering the sufficiently small error bars. The difference between sXR and sXR-NaCl in FE, which is defined as "V_{ini} for sXR or sXR-NaCl divided by V_{ini} for free ZS-XR", is smaller than that in V_{ini}. Nevertheless, Figure 6c suggests that FE for sXR-NaCl is smaller than FE for sXR.

We then discuss the effects of salt concentration and species of salt ions. The salt addition could influence the enzymatic reactions through a variety of rather complex mechanisms. However, as far as the screening of negative charges on the DNA surface is concerned, it is performed by not anions but cations. Hence, the screening effect can be dependent only on cation species and it becomes larger as the cation concentration increases. As a matter of fact, we tested CsCl as well as NaCl at two different concentrations, 0.5 and 1 M for enzyme reactions occurring for sXR[17] (Figure S18). The initial reaction velocity V_{ini} is chosen as the most important parameter. We obtained experimental data showing that the screening effect is larger and V_{ini} is slower for a higher concentration of NaCl or CsCl as expected but there are no large differences between the results from the NaCl and CsCl additions (Figure S18). These results are in line with the following, generally known experimental evidence: When a physicochemical property (e.g., the thermal denaturation temperature of a protein) changes by addition of salt ions, the change for cations is smaller than that for anions, the change is less correlated with cation species than with anion species, and the effect of cations is more difficult to interpret than that of anions.[56]

3.7. Substrate Concentrations Near a Free Enzyme and Near an Enzyme Assembled in the Vicinity of the DNA Surface. The local concentration (i.e., the concentration near a surface or within the space confined between two surfaces) of a substrate in the system is determined by the interplay of energetic and entropic effects. Energetically, the substrate concentration at a local position is closely related to the number density of water molecules in it. For instance, there is a strong tendency for a substrate with a high energetic affinity for water to be hydrated in a site where the number of water molecules contacting the substrate is maximized. On the other hand, a substrate is entropically driven to contact the free enzyme surface, or both the enzyme and DNA scaffold surfaces as explained in a later paragraph.

We compare the substrate concentration near a free enzyme with that near an enzyme assembled close to the DNA surface. They depend on the number density of water surrounding the substrate and the energetic affinity (hereafter, the energetic affinity is referred to simply as the "affinity") of the substrate for water. When the substrate concentration near an enzyme close to the DNA surface is higher or lower than that near the free enzyme surface, the enzyme reaction is accelerated or decelerated, resulting in increased or decreased enzyme activity.

First, we discuss the average number densities of water in the bulk, near a free enzyme, and near the DNA surface, denoted by C_{W1}, C_{W2}, and C_{W3}, respectively. The surfaces of the XR and CA enzymes consist of positively charged, negatively charged, polar, and nonpolar groups which are almost randomly mixed. The effective surface charge density represented by the total charge divided by the water-accessible surface area is dependent on the pH of the enzyme reaction buffer (Figure S19), but almost zero in our experiments. Nevertheless, the number density of water molecules is slightly higher near an enzyme surface than in the bulk due to the following entropic effect. The enzyme generates an EV for the water molecules in the system. Each water molecule also generates an EV for the

https://doi.org/10.1021/acsami.4c18192
ACS Appl. Mater. Interfaces 2025, 17, 15775−15792

other water molecules. When a water molecule contacts the enzyme surface, the EVs overlap, and the total volume available for the translational displacement of the other water molecules increases by the overlapping volume, leading to an entropic gain of the other water molecules. This is the entropic effect driving each water molecule to contact the enzyme surface: $C_{W1} \sim C_{W2}$ but $C_{W1} < C_{W2}$ in a strict sense. (If a surface consists of nonpolar groups alone, it is likely that a low-density layer of water is formed near the surface.[57]) As a matter of fact, it has also been pointed out by experimental and MD simulation studies[58,59] that the number density of the first hydration layer of water molecules near a protein is, on the average, slightly higher than that of bulk water even when the total charge of the protein is zero. On the other hand, as described in "High-density water layer on the DNA scaffold surface" (Note S3), due to the energetic effect, the number density of water molecules near the DNA surface is, on the average, much higher than that near the enzyme surface: $C_{W2} \ll C_{W3}$. Taken together, we obtain the following relationships obtained: $C_{W1} < C_{W2} \ll C_{W3}$.

Here, our discussion is focused on the energetic effect. An important parameter is the number of water molecules that can come into contact with a substrate, M. M is closely related to the affinity of the substrate for water. For a substrate in bulk water, $C_{W1} < C_{W2}$ (Figure 7a), but when a substrate contacts the enzyme surface (Figure 7b), there is a region where water molecules cannot enter, resulting in $M_{(b)} < M_{(a)}$. Here $M_{(b)}$ and $M_{(a)}$ denote M for the substrate in (b) and M for the free substrate in the bulk water (a), respectively. On the other hand, $M_{(c)} > M_{(a)}$ even in the presence of a region that water molecules cannot enter because $C_{W1} \ll C_{W3}$. Taken together, we obtain the following relationship: $M_{(c)} > M_{(a)} > M_{(b)}$.

Our principal concern is the concentrations of the substrates with high and low affinities for water in (b) and (c), respectively. The substrates behave in accordance with the structure of the water molecules formed near the surface of enzyme and/or DNA. The system is energetically more stable when the substrate with a high affinity for water is in (a) than in (b), whereas the opposite is true for substrates with a low affinity. In other words, a substrate with a high affinity for water prefers to be hydrated in bulk water rather than to come into contact with the free enzyme. In contrast, a substrate with a low affinity for water is excluded by water from the bulk to the enzyme surface. Because $M_{(c)} > M_{(b)}$, the system is energetically more stable when the substrate with high affinity is in (c) than in (b), whereas the opposite is true for the substrate with low affinity. We have classified substrates with high and low affinities for water (Figure 4b, $\mu_w = -6.30$ kcal/mol) as hydrophilic and hydrophobic substrates, respectively. This is reasonable because in the present case, the hydration free energy of each substrate is primarily determined by its affinity (we emphasize that this is the energetic affinity) for water. Important orders are $C_{hydrophilic,(c)} > C_{hydrophilic,(b)}$ and $C_{hydrophobic,(b)} > C_{hydrophobic,(c)}$ where the difference, which increases with increasing hydrophilicity or hydrophobicity of the substrate, can be quite large. Here, $C_{hydrophilic,(a)}$, is the concentration of the hydrophilic substrate in bulk water (a).

The above discussion is focused on the energetic effect. As for the entropic effect, although it should be smaller than the energetic effect in the present case, substrates are driven to contact the enzyme and DNA surfaces for the following reason:[22] each enzyme and DNA nanostructure generates an excluded volume (EV) that is inaccessible to the centers of the water molecules in the system. When a substrate contacts one or both of the enzyme and DNA surfaces, the EVs overlap, and the total volume available for the translational displacement of water molecules increases by the overlapping volume, resulting in a water-entropy gain. The overlapping volume and the water-entropy gain are much greater when the substrate is in contact of with both surfaces. This entropic effect makes the difference in $C_{hydrophilic,(c)} > C_{hydrophilic,(b)}$ larger, whereas it makes the difference in $C_{hydrophobic,(b)} > C_{hydrophobic,(c)}$ smaller.

Theoretical studies using ADIET have shown that solutes with low affinity for water are largely enriched near a surface with low surface charge density, but the degree of enrichment decreases with increasing surface charge density.[52] Let us consider the behavior of multiple components (including the water molecule) near a surface in aqueous solution. When one component is highly enriched near the surface due to a certain physical factor, another component with a high affinity for the enriched component will also be enriched near the surface, as has been shown both experimentally and theoretically.[60] These two components correspond to water and a substrate with relatively higher energetic affinity (D-xylose, D,L-GA, 4-NBA, and *p*-NPA).

3.8. Effect of Local Substrate Concentration on Catalytic Enhancement of an Enzyme on a DNA Scaffold Compared to Free Enzyme in Bulk Solution.

In Figure 5, the thickness of the dense layer of water molecules near the DNA surface is only ~1 nm.[51] On the other hand, the separation between the enzyme and the DNA surfaces in our experiments fluctuates to a large extent within a range of 0−5.5 nm (Figure S3). When the separation was large enough, the substrate concentration around the enzyme in (c) was the same as that around the free enzyme. The presence of the DNA surface only affects the substrate concentration near a portion of the enzyme. The position of the active site of the enzyme was also variable. Taken together, enzyme activity is modulated only when the active site of the enzyme is sufficiently close to the DNA surface, and this modulation occurs only intermittently. However, when the differences between $C_{hydrophilic,(c)}$ and $C_{hydrophilic,(b)}$ and between $C_{hydrophobic,(c)}$ and $C_{hydrophobic,(b)}$ are large, the observed FE becomes larger or smaller than 1.

Interestingly, in contrast to the present result of sCA, the FE of CA on the other type of DNA scaffold was almost equal to 1 when a single molecule of ZS-CA was assembled in each cavity of the planar-like DNA origami scaffold (Figure S20a).[22] These results strongly suggest that the high-density water layer on the inner surface of the hexagonal prism, which is not present in the cavity of the planar DNA scaffold, plays a role in enhancing the catalytic reaction rate of sCA by increasing the local concentration of the substrate *p*-NPA near the DNA surface. Similarly, the effect of the high-density water layer on the inner surface of the hexagonal prism explains the result of our recent report that the efficiency of the enzymatic cascade reaction of XR and XDH in the hexagonal prism DNA scaffold is higher than that in the cavity of the planar DNA scaffold, even when the interenzyme distance between XR and XDH is comparable (Figure S19b and S19c).[61] Xylitol, a substrate for XDH produced from D-xylose by the first enzyme XR, is hydrophilic and is enriched in the high-density layer of water formed near the DNA surface. Based on the difference in the geometric properties of the DNA surface between the hexagonal prism and the cavity, we can expect that the time during which the active site of XDH remains sufficiently close to the DNA

https://doi.org/10.1021/acsami.4c18192
ACS Appl. Mater. Interfaces 2025, 17, 15775−15792

surface should be longer in the hexagonal prism, leading to higher efficiency of XR/XDH cascade reaction on the floor of the hexagonal prism.[21,61]

In the case of XR, K_m for the substrate D-xylose is much higher than K_m for the cofactor NADH.[40] Let C_m be the D-xylose or NADH concentration required for the reaction velocity to reach half of the maximum reaction velocity. The difference between D-xylose and NADH in K_m shows that C_m for D-xylose is much higher than C_m for NADH. This result suggests that the enzyme activity is more influenced by the D-xylose concentration than by the NADH concentration. Therefore, it can be rationalized that FE is discussed by looking at the substrates with the assumption that FE is not significantly affected by the local concentration of NADH (see Note S5).

3.9. Comments on a Previously Reported Interpretation of the Catalytic Enhancement of Enzymes by the DNA Nanostructure. Zhao et al. reported a series of interesting results on the enhancement of enzyme activity by using a DNA nanostructure and provided an interpretation.[16] They attributed the enhanced enzyme activity to the negative, high surface charge density of the DNA surface. They also showed that the degree of enhancement decreased with the addition of NaCl. Our interpretation is similar in both of these respects. However, the following points described by them are controversial. (1) It is hypothesized that the entire enzyme is immersed in a highly ordered, hydrogen-bonded water environment created by the presence of the DNA surface. (2) In this water environment, the enzyme structure was more stable, resulting in enhanced enzyme activity.

We first comment on point (1). The thickness of the water layer, whose structure and properties differ from those of the bulk, is only ∼1 nm.[51] Therefore, only a part of the enzyme is affected by the water layer. The most important feature of the water layer is its high density of water molecules. In the immediate vicinity of a solute with a high net charge or a highly charged surface, such as the DNA surface, a large percentage of water−water hydrogen bonds are broken owing to the preferential orientation of the dipole moments in the water molecules toward the solute or surface.[51,62,63] The hypothesis made in point (1) is not justified.

Concerning point (2), they claimed that the enzyme structure becomes more stable for the following reason: the highly ordered, hydrogen-bonded water is entropically unstable, and the amount of such unstable water increases upon enzyme unfolding; thus, the formation of highly ordered hydrogen-bonded water prevents the enzyme from unfolding to a greater extent. Even when the enzyme was immersed in such a water environment, point (2) could not be rationalized. Kinoshita et al. showed that the entropic loss upon protein unfolding related to the water near the protein is much less important than the loss of translational configurational entropy of water in the entire system.[62,64−67] Therefore, the enzyme structure is not stabilized by highly ordered hydrogen-bonded water. Even if stabilization did occur, it would not always result in enhanced enzyme activity without specific stabilization of the transition state in the chemical reaction. Furthermore, point (2) contradicts the lower reaction velocity observed for hydrophobic substrates in our experiments.

We emphasize that our experimental observations can be explained not by the interpretation of Zhao et al. but by our own interpretation. According to the interpretation of Zhao et al., the enzymatic reactions are always accelerated near the DNA surface due to the enhanced stability of the enzyme structure, which is in contrast to our experimental observations. Our results show that they are accelerated for hydrophilic substrates but decelerated for hydrophobic substrates. Their results of activity enhancement for GOx, HRP, glucose-6-phosphate dehydrogenase, malic dehydrogenase and lactic dehydrogenase upon encapsulation in DNA cages are well explained by our interpretation by considering the hydrophilic character of the substrates for these enzymes. Their finding of an inverse correlation between increased activity and size of the encapsulated enzyme actually supports our interpretation on the role of the high-density water layer is formed near the DNA nanostructure. A smaller-sized enzyme should have a higher frequency of immersing the active site of the enzyme in a high-density layer of water than the larger size enzyme, resulting in a greater enhancement of the reaction rate.

3.10. Consistency between Our Experimental Observations and Our Hypothesis. Since the results of our experiments and theoretical analyses suggest that the FE for the substrate is better correlated with ε of the substrate than with S (ε and S are the energetic and entropic components of the hydration free energy μ ($\mu = \varepsilon - TS$), respectively), the affinity of the substrate for water can be discussed in terms of the energetic affinity which is referred to simply as the "affinity" below. For common chemical reactions catalyzed by free enzymes in bulk aqueous solution, the reaction rate increases or decreases as the substrate concentration increases or decreases. When a high-density layer of water is formed near the DNA nanostructure, hydrophilic substrates with high affinity for water are enriched within the layer, while hydrophobic substrates with low affinity for water are excluded from the layer (i.e., somewhat depleted within the layer). Importantly, the active sites of enzymes near the DNA nanostructure are intermittently immersed in the layer. As a result, the *effective* concentration of hydrophilic substrates becomes higher, while that of hydrophobic substrates becomes lower. Therefore, when the enzymes are placed near the DNA nanostructure, the chemical reaction is accelerated for hydrophilic substrates and decelerated for hydrophobic substrates. With the addition of NaCl, the negative charges on the DNA surface are screened, and the effect of the formation of the high-density layer of water becomes weaker, so the degree of acceleration or deceleration described above becomes smaller (Figure 6). In addition, the screening effect becomes larger as the NaCl concentration increases. This hypothesis, supported by our accurate statistical mechanics calculations of hydration properties of the substrates, can explain all our experimental observations quite consistently: This is the novelty of our study.

Our experimental result of increased or decreased enzyme activity cannot be explained by the electrostatic interaction between the DNA scaffold surface and a substrate, nor by the lower local pH modulated by the surface. If the effect of the electrostatic interaction were dominant, the enzyme activity would increase only for substrates with positive total charges, because the charge density of the DNA surface is negative. We note that we use substrates with zero total charge. Nevertheless, the enzyme activity increases or decreases depending on the hydration properties of the substrates. Our experimental result also cannot be explained by the effect of the lower local pH, which was justified by the finding in our previous work that an almost 4-fold increase in reaction velocity was observed

https://doi.org/10.1021/acsami.4c18192
ACS Appl. Mater. Interfaces 2025, 17, 15775−15792

for both cases of XR and XDH assembled on the DNA scaffold compared to the respective free enzymes even XR and XDH have different pH preferences, at pH 6 and 8, respectively, and the charge of their substrates is neutral.[17] We then revisit the effect of enzyme adsorption on reaction vessel. FE is greater than 1 under the influence of adsorption, but the fact that FE is less than 1 for hydrophobic substrates clearly indicates that factors other than adsorption dominate the reaction. Since adsorption obviously does not occur for substrates but for enzymes, one or more factors other than adsorption must dominate for hydrophilic substrates to make FE greater than 1. Particular attention should be paid to Figure 4b. As shown in the Figure 4b, the fold enhancement (FE) for hydrophobic substrates is less than 1, indicating that the apparent enzyme activity decreases and there is another physical factor coming into play which predominates over the enzyme adsorption to the surface of reaction vessel. As explained above, this physical factor is the formation of the high-density layer of water near the DNA nanostructure. This predominance should also hold true for hydrophilic substrates because it is not a substrate but an enzyme that is adsorbed on the surface of reaction vessel.

The FE is not very different from 1 for the following reason: As mentioned above, the active sites of enzymes near the DNA nanostructure are only intermittently immersed in the high-density layer of water due to the large fluctuation of the separation between the enzyme and DNA nanostructure surfaces. If the fluctuation could be suppressed, the FE for hydrophilic substrates would become much higher than 1 and that for hydrophilic substrates would become much lower than 1. Pending the development of a technique to suppress the fluctuation, we show that the enzyme activity can be remarkably modulated (increased or decreased) when enzymes are fixed near a surface, depending on the surface and substrate properties.

If the surface is nonpolar unlike the DNA surface, it is likely that a low-density layer of water is formed near the surface[57] and hydrophilic substrates are depleted but hydrophobic substrates are enriched near the surface, leading to the decreased and increased enzyme activities for hydrophilic and hydrophobic substrates, respectively (FE < 1 for hydrophilic substrates and FE > 1 for hydrophobic substrates), which is opposite to the result reported in this manuscript. We believe that this statement is not specific to the enzymes and substrates studied. As for a hydrophobic substrate, an important factor is the following: When the surface possesses high surface-charge density, a high-density layer of water is formed near the surface, and a hydrophobic substrate with low affinity for water is depleted near the surface, leading to a decrease in the enzyme activity; when the surface is nonpolar, on the other hand, a low-density layer of water is formed near the surface, and a hydrophobic substrate with low affinity for water is enriched near the surface (or excluded from bulk water to the surface), leading to an increase in the enzyme activity.

A question then arises: to which of the hydrophilic and hydrophobic substrates does a given substrate belong? The correct answer can be given not by the sign of Log P or the hydration free energy of the substrate, but by determining whether the hydration free energy of the substrate is lower or higher than that of a water molecule using our accurate statistical mechanics theory[18] of hydration of a polyatomic solute.

3.11. Prospects for Potential Applications of Our Hypothesis to Biocatalytic Systems or Other Biomolecular Surfaces. Enzyme activity changes when the enzymes are located in the vicinity of the DNA nanostructure. In this study, we highlight the dependence of the change on the hydration properties of the substrates and provide original insights into the origin of the acceleration of the reaction for DNA-scaffolded enzymes compared to the corresponding free enzymes. It should be noted that the same enzyme is used for both free and scaffolded cases. Therefore, even for an enzyme other than XR and CA, the qualitative aspects of our conclusions regarding the change in enzyme activity are unlikely to change.

Water molecules are attracted to the surface by the electrostatic interaction between the surface and the dipole moment in a water molecule, resulting in the formation of a high-density layer of water near the surface. This result was obtained using not only a statistical mechanics theory[68] but also an MD simulation.[69] Taken together, it is clear that a high-density layer of water is formed near a surface with a high surface charge density or generating a strong electric field, regardless of its sign (negative or positive). This suggests a novel role for cellular scaffolds, such as lipid membranes, scaffold proteins, or proteins and/or nucleic acids in the liquid−liquid phase separation state, in modulating the local concentrations of substrates and ligands, which in turn control the efficiency of enzymatic reactions and ligand−receptor complex formation. Furthermore, the results can be extended to the general case of biocatalysts, where the rates of chemical reactions occurring near a surface in an aqueous environment can differ substantially from those in the bulk, depending on the surface properties and the affinity of the reactants for water.

A variety of scaffolds and supports, including proteins,[70] nucleic acids,[71] graphene oxide,[72] or metal−organic frameworks (MOFs)[73−75] have been used as enzyme scaffolds and applied in the construction of biomimetic systems. Immobilization of enzymes on biomaterials[71] and in MOFs[73−75] resulted in enhanced stability and enzyme activity. The mechanisms of the enhancement are to be elucidated in further studies. However, on the basis of the results of our study in the present article, we can suggest possible mechanisms.

In the MOF systems 1[73] and 2,[74] the enzyme and the substrate are GOx and glucose, respectively. The two systems share the feature that an enzyme molecule is surrounded by the MOF surface, which can be considered as rather hydrophilic. The surface properties of GOx should be similar to those of XR and CA considered in our study. Glucose is highly hydrophilic. First, we note that the average number density of water molecules near a protein surface is slightly higher than that in the bulk, as mentioned above, but that within the domain confined between a protein and a rather hydrophilic surface is significantly higher, leading to an enrichment of hydrophilic solutes within the confined domain. Systems 1 and 2 can be characterized as follows. (1) The hydrophilicity of the MOF surface is much lower than that of the DNA surface: Therefore, the average number density of water molecules within the surface-induced layer is also much lower. (2) In our case, as mentioned above, only a rather small part of the enzyme molecule comes in contact with the surface-induced high-density water layer. Moreover, the contact is only intermittent. In systems 1 and 2, by contrast, a much larger portion of the enzyme molecule is expected to be in continuous contact with the high-density water layer. As a result of point (2), the *effective* concentration of substrate for

https://doi.org/10.1021/acsami.4c18192
ACS Appl. Mater. Interfaces 2025, 17, 15775−15792

the scaffolded enzyme is significantly higher than that for the free enzyme, despite point (1), leading to the enhanced enzyme activity.

There is another report in the literature that when molecules of cytochrome *c*, enzymes, are embedded in surface region of ZIF-8, an MOF (system 3), the enzyme activity becomes about 10 times higher.[75] This intriguing result can be interpreted as follows. It can be assumed that the surfaces of ZIF-8 and cytochrome *c* are weakly hydrophilic and hydrophobic, respectively. More importantly, the substrate used, *tert*-butylhydroperoxide, is hydrophobic. In this system, unlike in systems 1 and 2, a high-density layer of water is not formed, and the details of the mechanisms coming into play are different. Suppose a surface is immersed in water or an aqueous solution. Unless the surface is highly hydrophilic (e.g., if the surface is only weakly hydrophilic or rather hydrophobic), hydrophobic solutes are excluded from the bulk to the surface, with the result that they are largely enriched near the surface. The enrichment increases with the solute hydrophobicity, the solute concentration in the bulk, or the hydrophobicity of the surface. The solute concentration near the surface can be much higher (e.g., an order of magnitude higher) than that in the bulk. These results, reported by Kinoshita[52] based on his statistical mechanics analyses, can be described as follows: Even if the solubility of a solute in bulk water is quite low, that in water near the surface can be much higher. It follows that the *effective* concentration of the substrate for the aforementioned enzyme can be an order of magnitude higher than that for the free enzyme. We note that the enrichment of hydrophobic substrates within a domain near a hydrophobic surface or confined between two hydrophobic surfaces can be much stronger than that of hydrophilic substrates within the high-density layer of water highlighted in our study.

The surface-induced effects derived from the scaffolds and supports provide clues to the functional expression of biocatalysts. Though we focus on systems where the high-density layer of water at the interface plays important roles, our findings provide physical and chemical insights into other systems as well. In general, the structure and properties of aqueous solution (in particular, the density profile of water molecules and the concentration profile of solutes) near a surface are substantially different from those in the bulk. Those confined between two surfaces exhibit further differences. Moreover, these differences are quite variable depending on hydration properties of the surfaces and solutes (e.g., the affinity of the surfaces and solutes for water). Our study sheds light on the elucidation of the surface-induced effects relevant to the activity enhancement of biocatalysts.

The surface-induced effect derived from the scaffolds and supports remains to be elucidated. Further investigation of the properties of the water layer at the interface of enzymes and these supports by MD or other methods would shed light on whether our finding on the role of a high-density water layer at the interface could apply to these supports.

4. CONCLUSIONS

By testing a variety of substrates with XR and CA possessing different catalytic mechanisms, we experimentally and theoretically investigated the acceleration of the enzyme reaction observed when the enzyme was assembled on the DNA nanostructure. It was found that the substrates could be divided into two groups: group 1, where the reaction velocity was increased when the enzyme was assembled on the DNA nanostructure as previously reported, and group 2, where it was unexpectedly decreased. We analyzed the hydration properties of the substrates using our accurate statistical mechanics theory[18] to classify the substrates into two groups that behave as hydrophilic and hydrophobic substrates, respectively. Strikingly, hydrophilic and hydrophobic substrates categorized on the basis of hydration free energy coincide with groups 1 and 2, respectively, which were classified according to the above experimental observations. The energetic affinity of the substrate for water, represented by the substrate-water electrostatic energy normalized by the water-accessible surface area of the substrate, was identified as the key factor. For group 1, the substrate concentration near an enzyme close to the DNA surface was much higher than that near a free enzyme, whereas the opposite was true for group 2. This difference can be attributed to the formation of a dense layer of water molecules near the DNA surface with a high negative charge density.

In this study, it was shown that the essential factors are the surface properties such as the surface charge density, the density structures of water near a single surface and within a domain confined between two surfaces, and the hydration properties of the substrates exemplified by the hydration free energy and the substrate-water electrostatic interaction energy normalized by the water-accessible surface area of the substrate. We were also successful in explaining why the efficiency of the enzyme cascade reaction of XR and XDH in the hexagonal prism DNA scaffold is higher than that in the cavity of the planar DNA scaffold, even at the same interenzyme distance between XR and XDH, which was found in our earlier work.[61] This success can be useful to the control of enzyme reaction steps in metabolic pathways to overcome the unfavorable kinetic parameters of cascaded enzymes. We previously found that a single type of enzyme exerts enhanced activity in the packed state and proposed that the entropic force generated by water increases the substrate or cofactor concentration within the domain confined between the enzyme surfaces, thus accelerating the enzyme catalytic reaction.[22] The domain confined between enzyme surfaces provides a reasonable model of enzymes packed in bacterial microcompartments, such as the carboxysome, where enzymes internally form a dynamic liquid-like matrix of enzyme condensates.[76] Taken together with the insight presented here, such modulation of the local concentration of ligands depending on the local environment could externalize the heterogeneous distribution of a given ligand within the cell, which plays an important role in organizing the cellular chemical reactions.

■ ASSOCIATED CONTENT

Supporting Information

The Supporting Information is available free of charge at https://pubs.acs.org/doi/10.1021/acsami.4c18192.

Decomposition of hydration free energy of a solute into energetic and entropiccomponents under isochoric condition; Relationship of surface charge properties between double helix DNA and DNAnanostructure; High-density layer of water molecules near a negatively charged surface; Formation of a high-density layer of water near a surface with a high surface charge density; Note S5 Effect of the local concentration of a cofactor

https://doi.org/10.1021/acsami.4c18192
ACS Appl. Mater. Interfaces 2025, 17, 15775−15792

on the enhancement of the catalytic activity; Nucleotide sequences for the DNA staple strands containing the binding sites for enzyme with BG modification; Loading yield of ZS-XR on the DNA scaffold; Enzyme kinetic parameters; Loading yield of ZS-CA; Front view and blueprint modified from the caDNAno[12] software interface of a DNA scaffold with enzyme binding sites; Construction of the DNA scaffold; Assembly of enzyme on the DNA scaffold; AFM images of ZS-XR; Enzymatic reaction schemes of xylose reductase; The enzyme reactions of free ZS-XR with different enzyme concentrations.; Measurement of the enzyme kinetics of free ZS-XR for xylose; AFM images of ZS-CA assembled on DNA scaffold with three binding sites; Enzyme reaction schemes of carbonic anhydrase with various substrates; The effect of NaCl on the reaction of free ZS-XR or sXR; Color mapping for enzyme surface by atomic charge; ZS-CA in the cavities of planar-like DNA scaffold; References (PDF)

AUTHOR INFORMATION

Corresponding Author

Takashi Morii − *Institute of Advanced Energy, Kyoto University, Uji, Kyoto 611-0011, Japan; Department of Health and Nutrition, Kyoto Koka Women's University, Kyoto 615-0882, Japan;* orcid.org/0000-0003-3663-3267; Email: morii.takashi.68s@st.kyoto-u.ac.jp

Authors

Peng Lin − *Institute of Advanced Energy, Kyoto University, Uji, Kyoto 611-0011, Japan;* orcid.org/0000-0003-2601-0787

Tomohiko Hayashi − *Interdisciplinary Program of Biomedical Engineering, Assistive Technology, and Art and Sports Sciences, Faculty of Engineering, Niigata University, Niigata 950-2181, Japan*

Huyen Dinh − *Tam Anh Research Institute (TAMRI), Hochiminh City 72108, Vietnam;* orcid.org/0000-0003-0336-0362

Eiji Nakata − *Institute of Advanced Energy, Kyoto University, Uji, Kyoto 611-0011, Japan;* orcid.org/0000-0001-9564-6805

Masahiro Kinoshita − *Graduate School of Science, Chiba University, Chiba 263-8522, Japan; Center for the Promotion of Interdisciplinary Education and Research, Kyoto University, Kyoto 606-8501, Japan;* orcid.org/0000-0001-8060-045X

Complete contact information is available at: https://pubs.acs.org/10.1021/acsami.4c18192

Author Contributions

The manuscript was written through the contributions of all authors. All the authors approved the final version of the manuscript.

Funding

This work was supported by JSPS KAKENHI Grant Numbers 17H01213, 23H02083, 23K17977 and 23K26776 (T.M.), 20H02860, 22H05418 and 24K01629 (E.N.), 24K17787 (P.L.), and by the JST CREST Grant Number JPMJCR18H5 (T.M.), Japan.

Notes

The authors declare no competing financial interest.

ACKNOWLEDGMENTS

This work acknowledges the Collaboration Program of the Laboratory for Complex Energy Processes, Institute of Advanced Energy, Kyoto University (P.L.). This work acknowledges the Kyoto University Foundation (P.L.).

ABBREVIATIONS

GOx, glucose oxidase; HRP, horseradish peroxidase; XR, xylose reductase; XDH, xylitol dehydrogenase; CA, carbonic anhydrase; ZS-XR, modular adaptor ZF-SNAP-fused XR; ZS-CA, modular adaptor ZF-SNAP-fused CA; sXR, DNA-scaffolded ZS-XR; sCA, DNA-scaffolded ZS-CA; BG, benzylguanine; FE, catalytic fold enhancement; D,L-GA, D,L-glyceraldehyde; 4-NBA, 4-nitrobenzaldehyde; Ethyl BF, ethyl benzoylformate; *o*-CAP, *o*-chloroacetophenone; *p*-NPA, *p*-nitrophenyl acetate; *p*-NPB, *p*-nitrophenyl butyrate; *p*-NPV, *p*-nitrophenyl valerate; ADIET, angle-dependent integral equation theory; WAS, water-accessible surface; EV, excluded volume

REFERENCES

(1) Agapakis, C. M.; Boyle, P. M.; Silver, P. A. Natural strategies for the spatial optimization of metabolism in synthetic biology. *Nat. Chem. Biol.* **2012**, *8*, 527−535.

(2) Kastritis, P. L.; Gavin, A. C. Enzymatic complexes across scales. *Essays Biochem.* **2018**, *62*, 501−514.

(3) Liu, L. N. Distribution and dynamics of electron transport complexes in cyanobacterial thylakoid membranes. *Biochim. Biophys. Acta, Bioenerg.* **2016**, *1857*, 256−265.

(4) Laursen, T.; Lam, H. Y. M.; Sørensen, K. K.; Tian, P.; Hansen, C. C.; Groves, J. T.; Jensen, J. T.; Christensen, S. M. Membrane anchoring facilitates colocalization of enzymes in plant cytochrome P450 redox systems. *Commun. Biol.* **2021**, *4*, No. 1057.

(5) Bonacci, W.; Teng, P. K.; Afonso, B.; Niederholtmeyer, H.; Grob, P.; Silver, P. A.; Savage, D. F. Modularity of a carbon-fixing protein organelle. *Proc. Natl. Acad. Sci. U.S.A.* **2012**, *109*, 478−483.

(6) Du, P.; Xu, S.; Xu, Z. K.; Wang, Z. G. Bioinspired self-assembling materials for modulating enzyme functions. *Adv. Funct. Mater.* **2021**, *31*, No. 2104819.

(7) Rothemund, P. W. K. Folding DNA to create nanoscale shapes and patterns. *Nature* **2006**, *440*, 297−302.

(8) Zhan, P.; Peil, A.; Jiang, Q.; Wang, D.; Mousavi, S.; Xiong, Q.; Shen, Q.; Shang, Y.; Ding, B.; Lin, C.; Ke, Y.; Liu, N. Recent advances in DNA origami-engineered nanomaterials and applications. *Chem. Rev.* **2023**, *123*, 3976−4050.

(9) Ellis, G. A.; Klein, W. P.; Lasarte-Aragonés, G.; Thakur, M.; Walper, S. A.; Medintz, I. L. Artificial Multienzyme Scaffolds: Pursuing in Vitro Substrate Channeling with an Overview of Current Progress. *ACS Catal.* **2019**, *9*, 10812−10869.

(10) Jaekel, A.; Stegemann, P.; Saccà, B. Manipulating enzymes properties with DNA nanostructures. *Molecules* **2019**, *24*, 3694.

(11) Lin, J. L.; Wheeldon, I. Kinetic enhancements in DNA-enzyme nanostructures mimic the Sabatier principle. *ACS Catal.* **2013**, *3*, 560−564.

(12) Gao, Y.; Roberts, C. C.; Zhu, J.; Lin, J. L.; Chang, C. E. A.; Wheeldon, I. Tuning enzyme kinetics through designed intermolecular interactions far from the active site. *ACS Catal.* **2015**, *5*, 2149−2153.

(13) Kosinski, R.; Perez, J. M.; Schöneweiß, E. C.; Ruiz-Blanco, Y. B.; Ponzo, I.; Bravo-Rodriguez, K.; Erkelenz, M.; Schlücker, S.; Uhlenbrock, G.; Sanchez-Garcia, E.; Saccà, B. The role of DNA nanostructures in the catalytic properties of an allosterically regulated protease. *Sci. Adv.* **2022**, *8*, No. eabk0425.

(14) Timm, C.; Niemeyer, C. M. Assembly and purification of enzyme-functionalized DNA origami structures. *Angew. Chem., Int. Ed.* **2015**, *54*, 6745−6750.

(15) Zhang, Y.; Tsitkov, S.; Hess, H. Proximity does not contribute to activity enhancement in the glucose oxidase-horseradish peroxidase cascade. *Nat. Commun.* **2016**, *7*, No. 13982.
(16) Zhao, Z.; Fu, J.; Dhakal, S.; Johnson-Buck, A.; Liu, M.; Zhang, T.; Woodbury, N. W.; Liu, Y.; Walter, N. G.; Yan, H. Nanocaged enzymes with enhanced catalytic activity and increased stability against protease digestion. *Nat. Commun.* **2016**, *7*, No. 10619.
(17) Lin, P.; Dinh, H.; Morita, Y.; Zhang, Z.; Nakata, E.; Kinoshita, M.; Morii, T. Evaluation of the role of the DNA surface for enhancing the activity of scaffolded enzymes. *Chem. Commun.* **2021**, *57*, 3925−3928.
(18) Hayashi, T.; Kawamura, M.; Miyamoto, S.; Yasuda, S.; Murata, T.; Kinoshita, M. An accurate and rapid method for calculating hydration free energies of solutes including small organic molecules, peptides, and proteins. *J. Mol. Liq.* **2024**, *406*, No. 124989.
(19) Douglas, S. M.; Bachelet, I.; Church, G. M. A logic-gated nanorobot for targeted transport of molecular payloads. *Science* **2012**, *335*, 831−834.
(20) Amir, Y.; Ben-Ishay, E.; Levner, D.; Ittah, S.; Abu-Horowitz, A.; Bachelet, I. Universal computing by DNA origami robots in a living animal. *Nat. Nanotechnol.* **2014**, *9*, 353−357.
(21) Ngo, T. A.; Nakata, E.; Saimura, M.; Morii, T. Spatially organized enzymes drive cofactor-coupled cascade reactions. *J. Am. Chem. Soc.* **2016**, *138*, 3012−3021.
(22) Dinh, H.; Nakata, E.; Mutsuda-Zapater, K.; Saimura, M.; Kinoshita, M.; Morii, T. Enhanced enzymatic activity exerted by a packed assembly of a single type of enzyme. *Chem. Sci.* **2020**, *11*, 9088−9100.
(23) Nakata, E.; Dinh, H.; Ngo, T. A.; Saimura, M.; Morii, T. A. modular zinc finger adaptor accelerates the covalent linkage of proteins at specific locations on DNA nanoscaffolds. *Chem. Commun.* **2015**, *51*, 1016−1019.
(24) Wang, J.; Wolf, R. M.; Caldwell, J. W.; Kollman, P. A.; Case, D. A. Development and testing of a general amber force field. *J. Comput. Chem.* **2004**, *25*, 1157−1174.
(25) Jakalian, A.; Bush, B. L.; Jack, D. B.; Bayly, C. I. Fast, efficient generation of high-quality atomic charges. AM1-BCC model: I. *Method. J. Comput. Chem.* **2000**, *21*, 132−146.
(26) Jakalian, A.; Jack, D. B.; Bayly, C. I. Fast, efficient generation of high-quality atomic charges. AM1-BCC model: II. Parameterization and validation. *J. Comput. Chem.* **2002**, *23*, 1623−1641.
(27) Case, D. A.; Ben-Shalom, I. Y.; Brozell, S. R.; Cerutti, D. S.; Cheatham, T. E., III; Cruzeiro, V. W. D.; Darden, T. A.; Duke, R. E.; Ghoreishi, D.; Gilson, M. K.; Gohlke, H.; Goetz, A. W.; Greene, D.; Harris, R.; Homeyer, N.; Huang, Y.; Izadi, S.; Kovalenko, A.; Kurtzman, T.; Lee, T. S.; LeGrand, S.; Li, P.; Lin, C.; Liu, J.; Luchko, T.; Luo, R.; Mermelstein, D. J.; Merz, K. M.; Miao, Y.; Monard, G.; Nguyen, C.; Nguyen, H.; Omelyan, I.; Onufriev, A.; Pan, F.; Qi, R.; Roe, D. R.; Roitberg, A.; Sagui, C.; Schott-Verdugo, S.; Shen, J.; Simmerling, C. L.; Smith, J.; SalomonFerrer, R.; Swails, J.; Walker, R. C.; Wang, J.; Wei, H.; Wolf, R. M.; Wu, X.; Xiao, L.; York, D. M.; Kollman, P. A. *Amber18*; University of California, San Francisco, 2018.
(28) Kusalik, P. G.; Patey, G. N. On the molecular theory of aqueous electrolyte solutions. I. The solution of the RHNC approximation for models at finite concentration. *J. Chem. Phys.* **1988**, *88*, 7715−7738.
(29) Kusalik, P. G.; Patey, G. N. The solution of the reference hypernetted-chain approximation for water-like models. *Mol. Phys.* **1988**, *65*, 1105−1119.
(30) Cann, N. M.; Patey, G. N. An investigation of the influence of solute size and insertion conditions on solvation thermodynamics. *J. Chem. Phys.* **1997**, *106*, 8165−8195.
(31) Kinoshita, M. Molecular origin of the hydrophobic effect: Analysis using the angle-dependent integral equation theory. *J. Chem. Phys.* **2008**, *128*, No. 024507.
(32) Roth, R.; Harano, Y.; Kinoshita, M. Morphometric Approach to the Solvation Free Energy of Complex Molecules. *Phys. Rev. Lett.* **2006**, *97*, No. 078101.
(33) Beglov, D.; Roux, B. Numerical solution of the hypernetted chain equation for a solute of arbitrary geometry in three dimensions. *J. Chem. Phys.* **1995**, *103*, 360−364.
(34) Kovalenko, A.; Hirata, F. Self-consistent description of a metal-water interface by the Kohn−Sham density functional theory and the three-dimensional reference interaction site model. *J. Chem. Phys.* **1999**, *110*, 10095−10112.
(35) Hayashi, T.; Oshima, H.; Harano, Y.; Kinoshita, M. Water based on a molecular model behaves like a hard-sphere solvent for a nonpolar solute when the reference interaction site model and related theories are employed. *J. Phys.: Condens. Matter.* **2016**, *28*, No. 344003.
(36) Koehl, P.; Akopyan, A.; Edelsbrunner, H. Computing the Volume, Surface Area, Mean, and Gaussian Curvatures of Molecules and Their Derivatives. *J. Chem. Inf. Model.* **2023**, *63*, 973−985.
(37) Nguyen, T. M.; Nakata, E.; Saimura, M.; Dinh, H.; Morii, T. Design of modular protein tags for orthogonal covalent bond formation at specific DNA sequences. *J. Am. Chem. Soc.* **2017**, *139*, 8487−8496.
(38) Nguyen, T. M.; Nakata, E.; Zhang, Z.; Saimura, M.; Dinh, H.; Morii, T. Rational design of a DNA sequence-specific modular protein tag by tuning the alkylation kinetics. *Chem. Sci.* **2019**, *10*, 9315−9325.
(39) Zhang, Z.; Nakata, E.; Dinh, H.; Saimura, M.; Rajendran, A.; Matsuda, K.; Morii, T. Tuning the reactivity of a substrate for SNAP-tag expands its application for recognition-driven DNA-protein conjugation. *Chem. - Eur. J.* **2021**, *27*, 18118−18128.
(40) Son, H. F.; Lee, S. M.; Kim, K. J. Structural insight into D-xylose utilization by xylose reductase from Scheffersomyces stipitis. *Sci. Rep.* **2018**, *8*, No. 17442.
(41) Xu, D.; Liu, X.; Guo, C.; Zhao, J. Methylglyoxal detoxification by an aldo-keto reductase in the cyanobacterium Synechococcus sp. PCC 7002. *Microbiology* **2006**, *152*, 2013−2021.
(42) Alan Davis, R.; DeRuiter, J. Comparison of the catalytic and inhibitory properties of Pachysolen tannophilus xylose reductase to rat lens aldose reductase. *Appl. Microbiol. Biotechnol.* **1992**, *37*, 109−113.
(43) Kratzer, R.; Leitgeb, S.; Wilson, D. K.; Nidetzky, B. Probing the substrate binding site of Candida tenuis xylose reductase (AKR2B5) with site-directed mutagenesis. *Biochem. J.* **2006**, *393*, 51−58.
(44) Gruber, C.; Krahulec, S.; Nidetzky, B.; Kratzer, R. Harnessing Candida tenuis and Pichia stipitis in whole-cell bioreductions of o-chloroacetophenone: stereoselectivity, cell activity, in situ substrate supply and product removal. *Biotechnol. J.* **2013**, *8*, 699−708.
(45) Dinh, H.; Nakata, E.; Lin, P.; Saimura, M.; Ashida, H.; Morii, T. Reaction of ribulose biphosphate carboxylase/oxygenase assembled on a DNA scaffold. *Bioorg. Med. Chem.* **2017**, *27*, No. 115120.
(46) Wambo, T. O.; Chen, L. Y.; Phelix, C.; Perry, G. Affinity and path of binding xylopyranose unto *E. coli* xylose permease. *Biochem. Biophys. Res. Commun.* **2017**, *494*, 202−206.
(47) IAPWS Industrial Formulation 1997 for the Thermodynamic Properties of Water and Steam. In *International Steam Tables*; Springer: Berlin, Heidelberg DOI: 10.1007/978-3-540-74234-0_3.
(48) Mobley, D. L.; Bayly, C. I.; Cooper, M. D.; Shirts, M. R.; Dill, K. A. Small molecule hydration free energies in explicit solvent: An extensive test of fixed-charge atomistic simulations. *J. Chem. Theory Comput.* **2009**, *5*, 350−358.
(49) Schneider, B.; Patel, K.; Berman, H. M. Hydration of the phosphate group in double-helical DNA. *Biophys. J.* **1998**, *75*, 2422−2434.
(50) Nakano, M.; Tateishi-Karimata, H.; Tanaka, S.; Tama, F.; Miyashita, O.; Nakano, S.; Sugimoto, N. Thermodynamic properties of water molecules in the presence of cosolute depend on DNA structure: a study using grid inhomogeneous solvation theory. *Nucleic Acids Res.* **2015**, *43*, 10114−10125.
(51) Torrie, G. M.; Kusalik, P. G.; Patey, G. N. Molecular solvent model for an electrical double layer: Reference hypernetted-chain (RHNC) results for solvent structure at a charged surface. *J. Chem. Phys.* **1988**, *88*, 7826−7840.

(52) Kinoshita, M. Water structure and phase transition near a surface. *J. Solution Chem.* **2004**, *33*, 661−687.
(53) Kominami, H.; Kobayashi, K.; Yamada, H. Molecular-scale visualization and surface charge density measurement of Z-DNA in aqueous solution. *Sci. Rep.* **2019**, *9*, No. 6851.
(54) Møller Sønderskov, S.; Hyldgaard Klausen, L.; Amland Skaanvik, S.; Han, X.; Dong, M. In situ Surface Charge Density Visualization of Self-assembled DNA Nanostructures after Ion Exchange. *ChemPhysChem* **2020**, *21*, 1474−1482.
(55) Ngo, T. A.; Dinh, H.; Nguyen, T. M.; Liew, F. F.; Nakata, E.; Morii, T. Protein adaptors assemble functional proteins on DNA scaffolds. *Chem. Commun.* **2019**, *55*, 12428−12446.
(56) Sedlák, E.; Stagg, L.; Wittung-Stafshede, P. Effect of Hofmeister ions on protein thermal stability: Roles of ion hydration and peptide groups? *Arch. Biochem. Biophys.* **2008**, *479*, 69−73.
(57) Huang, D. M.; Geissler, P. L.; Chandler, D. Scaling of hydrophobic solvation free energies. *J. Phys. Chem. B* **2001**, *105*, 6704−6709.
(58) Biedermannová, L.; Schneider, B. Hydration of proteins and nucleic acids: advances in experiment and theory. A review. *Biochim. Biophys. Acta Gen. Subj.* **2016**, *1860*, 1821−1835.
(59) Laage, D.; Elsaesser, T.; Hynes, J. T. Water dynamics in the hydration shells of biomolecules. *Chem. Rev.* **2017**, *117*, 10694−10725.
(60) Fukami, K.; Koda, R.; Sakka, T.; Ogata, Y.; Kinoshita, M. Electrochemical deposition of platinum within nanopores on silicon: Drastic acceleration originating from surface-induced phase transition. *J. Chem. Phys.* **2013**, *138*, No. 094702.
(61) Lin, P.; Dinh, H.; Morita, Y.; Nakata, E.; Morii, T. Dynamic Assembly of Cascade Enzymes by the Shape Transformation of a DNA Scaffold. *Adv. Funct. Mater.* **2023**, *33*, No. 2215023.
(62) Inoue, M.; Hayashi, T.; Hikiri, S.; Ikeguchi, M.; Kinoshita, M. Comparison based on statistical thermodynamics between globule-to-coil transition of poly (N-isopropylacrylamide) and cold denaturation of a protein. *J. Mol. Liq.* **2020**, *317*, No. 114129.
(63) Kinoshita, M.; Yoshidome, T. Molecular origin of the negative heat capacity of hydrophilic hydration. *J. Chem. Phys.* **2009**, *130*, No. 144705.
(64) Harano, Y.; Kinoshita, M. Translational-entropy gain of solvent upon protein folding. *Biophys. J.* **2005**, *89*, 2701−2710.
(65) Kinoshita, M. A new theoretical approach to biological self-assembly. *Biophys. Rev.* **2013**, *5*, 283−293.4.
(66) Oshima, H.; Kinoshita, M. Essential roles of protein-solvent many-body correlation in solvent-entropy effect on protein folding and denaturation: comparison between hard-sphere solvent and water. *J. Chem. Phys.* **2015**, *142*, No. 145103.
(67) Kinoshita, M.; Hayashi, T. Unified elucidation of the entropy-driven and -opposed hydrophobic effects. *Phys. Chem. Chem. Phys.* **2017**, *19*, 25891−25904.
(68) Bérard, D. R.; Kinoshita, M.; Cann, N. M.; Patey, G. N. Structure of the metal-aqueous electrolyte solution interface. *J. Chem. Phys.* **1997**, *107*, 4719−4728.
(69) Shelley, J.; Patey, G. N.; Bérard, D. R.; Torrie, G. M. Modelling and structure of mercury-water interfaces. *J. Chem. Phys.* **1997**, *107*, 2122−2141.
(70) McConnell, S. A.; Cannon, K. A.; Morgan, C.; McAllister, R.; Amer, B. R.; Clubb, R. T.; Yeates, T. O. Designed protein cages as scaffolds for building multienzyme materials. *ACS Synth. Biol.* **2020**, *9*, 381−391.
(71) Lin, P.; Yang, H.; Nakata, E.; Morii, T. Mechanistic Aspects for The Modulation of Enzyme Reactions on the DNA Scaffold. *Molecules* **2022**, *27*, 6309.
(72) Lin, P.; Zhang, Y.; Yao, G.; Huo, H.; Ren, H.; Wang, Y.; Wang, S.; Fang, B. Immobilization of formate dehydrogenase on polyethylenimine-grafted graphene oxide with kinetics and stability study. *Eng. Life Sci.* **2020**, *20*, 104−111.
(73) Xia, H.; Li, N.; Huang, W.; Song, Y.; Jiang, Y. Enzymatic cascade reactions mediated by highly efficient biomimetic quasi metal−organic frameworks. *ACS Appl. Mater. Interfaces* **2021**, *13*, 22240−22253.
(74) Wu, X.; Ge, J.; Yang, C.; Hou, M.; Liu, Z. Facile synthesis of multiple enzyme-containing metal−organic frameworks in a biomolecule-friendly environment. *Chem. Commun.* **2015**, *51*, 13408−13411.
(75) Lyu, F.; Zhang, Y.; Zare, R. N.; Ge, J.; Liu, Z. One-pot synthesis of protein-embedded metal−organic frameworks with enhanced biological activities. *Nano Lett.* **2014**, *14*, 5761−5765.
(76) Wang, H.; Yan, X.; Aigner, H.; Bracher, A.; Nguyen, N. D.; Hee, W. Y.; Long, B. M.; Price, G. D.; Hartl, F. U.; Hayer-Hartl, M. Rubisco condensate formation by CcmM in β-carboxysome biogenesis. *Nature* **2019**, *566*, 131−135.

https://doi.org/10.1021/acsami.4c18192
ACS Appl. Mater. Interfaces 2025, 17, 15775−15792